Macrophage-derived extracellular vesicles regulate skeletal stem/progenitor Cell lineage fate and bone deterioration in obesity

Chen He [a], Chen Hu [a], Wen-Zhen He [a], Yu-Chen Sun [a], Yangzi Jiang [b,c,d], Ling Liu [a], Jing Hou [a], Kai-Xuan Chen [a], Yu-Rui Jiao [a], Mei Huang [a], Min Huang [a], Mi Yang [a], Qiong Lu [e], Jie Wei [f,g,h,j], Chao Zeng [f,g,h,j], Guang-Hua Lei [f,h,i,j], Chang-Jun Li [a,i,j,*]

[a] Department of Endocrinology, Endocrinology Research Center, Xiangya Hospital of Central South University, Changsha, Hunan, 410008, China
[b] School of Biomedical Sciences, Institute for Tissue Engineering and Regenerative Medicine, Faculty of Medicine, The Chinese University of Hong Kong, Hong Kong SAR, China
[c] Center for Neuromusculoskeletal Restorative Medicine (CNRM), The Chinese University of Hong Kong, Hong Kong SAR, China
[d] Key Laboratory for Regenerative Medicine, Ministry of Education, School of Biomedical Sciences, Faculty of Medicine, The Chinese University of Hong Kong, Hong Kong SAR, China
[e] Department of Pharmacy, The Second Xiangya Hospital of Central South University, Changsha, Hunan 410011, China
[f] Department of Orthopaedics, Xiangya Hospital of Central South University, Changsha, Hunan, 410008, China
[g] Department of Epidemiology and Health Statistics, Xiangya School of Public Health, Central South University, Changsha, Hunan, 410008, China
[h] Hunan Key Laboratory of Joint Degeneration and Injury, Changsha, Hunan, 410008, China
[i] National Clinical Research Center for Geriatric Disorders, Xiangya Hospital, Central South University, Changsha, Hunan, 410008, China
[j] Key Laboratory of Aging-related Bone and Joint Diseases Prevention and Treatment, Ministry of Education, Xiangya Hospital, Central South University, Changsha, China

A R T I C L E   I N F O

A B S T R A C T

Obesity-induced chronic inflammation exacerbates multiple types of tissue/organ deterioration and stem cell dysfunction; however, the effects on skeletal tissue and the underlying mechanisms are still unclear. Here, we show that obesity triggers changes in the microRNA profile of macrophage-secreted extracellular vesicles, leading to a switch in skeletal stem/progenitor cell (SSPC) differentiation between osteoblasts and adipocytes and bone deterioration. Bone marrow macrophage (BMM)-secreted extracellular vesicles (BMM-EVs) from obese mice induced bone deterioration (decreased bone volume, bone microstructural deterioration, and increased adipocyte numbers) when administered to lean mice. Conversely, BMM-EVs from lean mice rejuvenated bone deterioration in obese recipients. We further screened the differentially expressed microRNAs in obese BMM-EVs and found that among the candidates, miR-140 (with the function of promoting adipogenesis) and miR-378a (with the function of enhancing osteogenesis) coordinately determine SSPC fate of osteogenic and adipogenic differentiation by targeting the Pparα-Abca1 axis. BMM miR-140 conditional knockout mice showed resistance to obesity-induced bone deterioration, while miR-140 overexpression in SSPCs led to low bone mass and marrow adiposity in lean mice. BMM miR-378a conditional depletion in mice led to obesity-like bone deterioration. More importantly, we used an SSPC-specific targeting aptamer to precisely deliver miR-378a-3p-overloaded BMM-EVs to SSPCs via an aptamer-engineered extracellular vesicle delivery system, and this approach rescued bone deterioration in obese mice. Thus, our study reveals the critical role of BMMs in mediating obesity-induced bone deterioration by transporting selective extracellular-vesicle microRNAs into SSPCs and controlling SSPC fate.

1. Introduction

Currently, one-third of the population worldwide is overweight, and one in ten are classified as obese. Obesity, a complex pathophysiological condition, induces multiple tissue and organ deterioration and obesity-related metabolic syndrome and has an enormous socioeconomic

---

burden [1–4]. In the past, obesity was believed to be a protective factor for bone mineral density (BMD), but data from epidemiological studies strongly suggest that obesity increases fracture risk despite a standard or high BMD [5–7]. An animal study also showed that high-fat diet-induced obesity promotes bone marrow adiposity and bone fragility [8]. Thus, understanding how bone health and obesity are related is imperative for public health.

Skeletal stem/progenitor cells (SSPCs) are the source of osteoblasts (bone-forming cells) and adipocytes in bone marrow, and the switch of SSPCs differentiation from osteoblasts to adipocytes induced by cues in the local microenvironment leads to low bone mass and marrow fat accumulation, a typical characteristic of obesity- and aging-related bone phenotypes [8–11]. Li et al. demonstrated that high-fat diet-induced obesity leads to SSPC senescence and differentiation switching [12]. Additionally, studies have reported that the epigenetic regulation of Prrx1-positive SSPCs also affects lineage fate switching during age-related bone deterioration [13,14]. Recently, Zou et al. reported that in adult mice, marrow adipocytes negatively regulate bone growth, and adipocyte ablation induces osteogenesis [15]. Adipocyte accumulation in the bone marrow during obesity impairs stem cell-based hematopoietic and bone regeneration [16]. Thus, clarifying the regulation of SSPC fate switching in obesity and preventing the switch of SSPCs from osteoblasts to adipocytes would have multiple protective effects on bone health.

Obesity-related diseases appear to be associated with chronic inflammation. The vital component of obesity-induced chronic inflammation is the accumulation of proinflammatory tissue macrophages. Macrophages that accumulate in obese adipose tissue and bone marrow secrete proinflammatory cytokines and extracellular-vesicle microRNAs to regulate metabolic disease [17–19]. Extracellular vesicles play important roles in intercellular and interorganismal communication. The natural constituents of extracellular vesicles help them efficiently deliver functional cargo with minimal immune clearance and minimal adverse reactions [20]. Extracellular vesicles capsulate functional microRNAs and prevent their degradation in the circulation, efficiently transferring enriched microRNA signals to recipient cells and subsequently regulating body health, such as bone health [21–24]. The contents of extracellular vesicles are altered in obese individuals, thereby affecting the function of nearby or distant tissue [17,18,25]. Peruzzi et al. reported that circulating extracellular vesicles in obese adolescents impair SSPC osteogenesis and favor adipogenesis [26]. Zhang et al. reported that miR-144-5p, an extracellular-vesicle microRNA released from bone marrow macrophages in type 2 diabetes patients, impairs bone fracture healing by targeting Smad1 [27]. Given the vital roles of macrophages and macrophage-secreted extracellular vesicles in obesity-induced chronic inflammation and disease, we hypothesize that bone marrow macrophage-derived extracellular vesicles (BMM-EVs) may regulate SSPC differentiation switching and bone deterioration in obesity and that BMM-EV-wrapped microRNAs are the major regulators of the adipogenesis/osteogenesis of SSPCs. However, the role that macrophage-derived extracellular vesicles play in bone deterioration and SSPC differentiation, the functional cargos within extracellular vesicles, and the underlying mechanism have yet to be defined.

Aptamers, also known as chemical antibodies, are oligonucleotides with a 3D structure generated based on the systematic evolution of ligands by exponential enrichment (SELEX) [28]. Aptamers, recognized as drug delivery vehicles, have been exploited to precisely guide drugs to specific cell types to enhance the efficacy and safety of therapeutic drugs. In 2004, the U.S. Food and Drug Administration (FDA) approved the first therapeutic aptamer to treat neovascular age-related macular degeneration [29]. Aptamer-guided drug delivery systems exhibit invaluable treatment potential. A previous study identified an SSPC-specific 40-base aptamer to precisely deliver antagomiR-188 into mouse SSPCs, providing a new strategy for treating age-related bone loss [14]. In addition to microRNAs, aptamer-guided tissue/cell-specific delivery systems effectively deliver extracellular vesicle-wrapped drugs

to bone [30–32]. Compared with traditional treatments, aptamer-guided extracellular-vesicle drug delivery systems have low immunogenicity, high permeability, and precision-targeting ability [33]. Recently, Luo et al. reported that bone marrow stromal cell-derived extracellular vesicles conjugated with modified SSPC-specific aptamers, which we previously used, could target bone and promote bone regeneration [30]. However, the application of aptamer-guided extracellular-vesicle drug delivery systems in the field of obesity-related diseases is still lacking.

Herein, we show for the first time that bone marrow macrophages (BMMs) in obese mice secrete microRNA-containing extracellular vesicles, which cause bone deterioration (decreased bone volume, bone microstructural deterioration, and increased adipocyte numbers) in lean mice. In contrast, the treatment of obese recipients with BMM-EVs from lean mice yielded rejuvenating effects and a robust increase in bone mass. We further found that miR-140 and miR-378a within obese BMM-EVs coordinately regulate SSPC function by targeting the Pparα-Abca1 axis. To our knowledge, we are the first to generate BMM miR-140 conditional knockout mice and report on the resistance of these mice to obesity-induced bone deterioration. Furthermore, we demonstrated that mice with SSPC miR-140 conditional overexpression or BMM miR-378a conditional depletion exhibit low bone mass and marrow adiposity. Overexpressing miR-378a using an aptamer-engineered extracellular-vesicle delivery system improved bone mass in obese mice. Overall, our findings provide potential therapeutic targets, and the approach exhibited temporal and spatial specificity, high stability, and a lack of immunogenicity for obesity-induced bone deterioration, filling a gap in the application of aptamer-engineered extracellular-vesicle delivery systems in the field of obesity-induced bone deterioration, even for obesity-related diseases, and shedding light on improving bone quality in clinically obese and overweight patients.

2. Materials and methods

2.1. Animals

All mice we used were in C57BL/6J background and were maintained in a standard, specific pathogen-free barrier of the Department of Animals Laboratory, Central South University. Mice fed a normal chow diet were designated as lean mice. Mice fed a high-fat diet (D12492, 60 % kcal fat, Wuhan BIOPIKE Bioscience Co. Ltd., Wuhan, China) for at least 8 weeks and weighed at least 38 g were designated as obese. All the experimental protocols were approved by the Animal Care and Use Committees of the Laboratory Animal Research Center at Xiangya Medical School of Central South University.

To generate BMMs miR-140 and miR-378a conditional knockout mice, mice with LoxP-flanked miR-140 and miR-378a allele (miR-140$^{flox/flox}$ mice and miR-378a$^{flox/flox}$ mice) were treated with an adeno-associated virus carrying macrophage F4/80 promoter and Cre recombinase, respectively. The miR-378a$^{flox/flox}$ mice (T007903, Gempharmatech) and miR-140$^{flox/flox}$ mice (T015270, Gempharmatech) were constructed from Gempharmatech, Jiangsu, China.

Prrx1-cre and miR-140 TG$^{flox/flox}$ were crossed to generate SSPCs conditional over-expression of miR-140-5p transgenic mice. Prrx1-cre mice were purchased from Jackson Laboratory, and the miR-140 TG$^{flox/flox}$ were constructed from Gempharmatech, Jiangsu, China. The CAG-LSL-Mir140-IRES-EGFP gene fragment, which includes a loxP-flanked "stop" sequence (a transcriptional termination element) was inserted into the Hipp11 site of mice using CRISPR/Cas9 technology. The targeted allele was microinjected into the fertilized eggs of C57BL/6J mice, and the fertilized eggs were then surgically transferred into pseudo-pregnant C57BL/6 dams. F0 generation mice were obtained, and then F0 positive mice were mated with C57BL/6J mice to obtain stable inheritance F1.

For the genotyping of miR-378$^{flox/flox}$ and miR-140$^{flox/flox}$, PCR primers were synthesized by TSINGKE. miR-378 5′arm forward, 5′-CACTTGCTGCCGTACTTTCACG-3′, miR-378 5′arm reverse, 5′-

CCAACTGACCTTGGGCAAGAACAT-3'; miR-378 3′arm forward, 5′-TACTCTTGCCGTTCATGTGCG-3′, miR-378 3′arm reverse, 5′-AAGATGGCTCCTACCAAAGGTAGC-3'; miR-140 forward, 5′-CGTGGA-CAACAGGCAGAG-3′, miR-140 reverse, 5′- ATGCCCACCAAGCACAGC-3'. For the genotyping of miR-140 TG^{flox/flox}, PCR primers were synthesized by TSINGKE. miR-140 WT forward, 5′-AGTCTTTCCCTTGCCTCTGCT-3′, and miR-140 WT reverse, 5′-GGGTCTTCCACCTTTCTTCAG-3'; miR-140 3′arm forward, 5′-CCTCCTCTCCTGACTACTCCCAGTC-3′, miR-140 3′arm reverse, 5′-TCACAGAAACCATATGGCGCTCC-3'; miR-140 5′arm forward, 5′-TCAGCGTTCAGACTCCTCAGAATGT-3′, miR-140 5′arm reverse, 5′-TCAATGGAAAGTCCCTATTGGCGT-3'.

2.2. Cell culture

Primary bone marrow mesenchymal stem cells (BMSCs) were isolated and cultured, as reported previously [34]. Briefly, bone marrow cells were flushed out from tibiae and femurs of 4-week-old mice and incubated with mouse Sca-1 (108108, Bio Legend), CD11b (101226, Bio Legend), CD29 (102206, Bio Legend), and CD45 (103132, Bio Legend) antibodies for 20 min at 4 °C. Then we performed fluorescence-activated cell sorting (FACS) and cultured the sorted CD29^+ Sca-1^+CD45^−CD11b^− BMSCs with α-MEM (BI) supplemented with 10 % FBS (Gibco), 100 U/mL penicillin, 100 μg/mL streptomycin (Hyclone).

For primary mouse bone marrow macrophage isolation, we flushed out and collected bone marrow cells from tibiae and femurs of mice in α-MEM and cultured them with α-MEM supplemented with 10 % FBS, 100 U/mL penicillin, 100 μg/mL streptomycin. After attachment for 12 h, the supernatant was collected and centrifuged, then grown in α-MEM supplemented with 10 % FBS, 100 U/mL penicillin, 100 μg/mL streptomycin, and 30 ng/ml M-CSF (Proteintech) for 3 days. All cultures were maintained at 37 °C with 5 % CO_2 in a humidified atmosphere.

2.3. Extracellular vesicle isolation, characterization, uptake

Extracellular vesicles were collected as previously described [35]. After being cultured in the extracellular vesicle-free medium for 72 h, the culture medium of BMMs was collected and centrifuged at 3000 g for 20 min to remove cells and cell debris; then the supernatant was filtered with 0.22 μm filter (Millipore). Next, centrifuge at 100, 000 g for 6 h at 4 °C. The extracellular vesicles were pelleted at the bottom of the tube.

Transmission electron microscopy was used to observe morphology, while NanoSight analysis was conducted to measure the size distribution and particle concentration. Western blotting analysis was performed using Tsg101 (ab125011, Abcam), CD9 (ab92726, Abcam), CD63 (ab217345, Abcam), and Calnexin (ab213243, Abcam) antibodies to identify extracellular vesicles.

The suspended extracellular vesicles were incubated with 1 mL Diluent C containing 4 μM PKH26 (sigma) for 5 min. Next, mix 1 ml 1 % bovine serum albumin with the labeling reaction system and incubate for 1 min to stop the labeling action. The extracellular vesicles were washed three times with cold PBS using an Amicon ultrafilter and resuspended in 200 μL PBS. These labeled extracellular vesicles were added 20 μg per 10^5 recipient cells to culture with SSPCs for 12 h and then labeled cytoskeleton using 50 mg/ml phalloidin to detect extracellular-vesicle trafficking.

2.4. miRNA microarray assay

To identify the differently expressed microRNAs in the extracellular vesicles released by BMMs from obese mice and lean mice, miRNA microarray assays were performed with the help of Obio Technology (Shanghai) Corp., Ltd.

2.5. microRNA transfection and Pparα lentiviruses infection

miR-378a mimic and miR-140 mimic was designed and produced by RiboBio Company. For transfection of miR-378a and miR-140 mimics, primary SSPCs and BMMs were seeded in 12-well plates and 100 mm cell culture dish, respectively, then transfected with these mimics for 4–6 h using lipofectamine 2000 (Invitrogen).

Pparα overexpression lentiviruses were designed and produced by HANBIO, Shanghai, China. For the overexpression of Pparα, SSPCs were seeded in 12-well plates and infected with Pparα overexpression lentiviruses according to the manufacturer's instructions.

2.6. microRNA-enriched macrophage extracellular vesicle isolation

Primary BMMs were seeded in a 100 mm cell culture dish and transfected with miR-378a mimic and miR-140 mimic for 4–6 h, respectively. miR-378a mimic and miR-140 mimic transfected BMMs were washed three times with PBS. Then, cultured in the extracellular vesicle-free medium for 72 h, the culture medium of miR-378a mimic and miR-140 mimic transfected BMMs were collected for further extracellular vesicle isolation.

2.7. Intramedullary injection of adeno-associated virus

Adeno-associated virus (AAV) is a modified natural single-stranded DNA virus, recognized as the most promising gene transfer vector. HBAAV2/2-F4/80-cre-ZsGreen (AAV-F4/80-cre-ZsGreen) was designed and produced by HANBIO, Shanghai, China. F4/80-cre overloaded adeno-associated virus and its control virus were packed in titers of 1.3–1.4*10^12 vg/ml. Mice were anesthetized with isoflurane, the skin was disinfected with 75 % alcohol, hair around the knee joint was shaved, and the knees were exposed sterile. Mice were randomly divided into two groups. Each mouse femur was injected with 30 μL AAV-F4/80-Cre-ZsGreen or control (AAC-NC-ZsGreen) using an insulin needle.

pAAV-CMV-EGFP-3xFLAG-miR-378a-3p-WPRE (AAV-miR-378a-3p-EGFP) was designed and produced by OBIO, Shanghai, China. Twenty-five microliter AAV-miR-378a-3p-EGFP (3.2×10^{12} vg/ml) was injected into the femurs using an insulin needle. The method of intramedullary injection was as described above.

2.8. Osteogenic and adipogenic differentiation

SSPCs were cultured in α-MEM supplemented with 10 % FBS, 100 U/mL penicillin, 100 μg/mL streptomycin, 0.1 mM dexamethasone (D1756, sigma), 10 Mm b-glycerol phosphate (G9422, sigma) and 50 mM ascorbate-2-phosphate (A4544, sigma) for 6-21 days for osteogenic differentiation, while adipogenic differentiation was cultured in adipogenic medium (cyagen) for 6-14 days. The culture medium was changed every three days.

2.9. qRT-PCR analysis

Total RNA from tissues or cultured cells was isolated using the TRIzol reagent, 1 μg total RNA was used to conduct mRNA reverse transcription using the PrimeScript RT reagent Kit (Takara), and 2 μg total RNA to perform microRNA reverse transcription using All-in-One™ miRNA Frist-Strand cDNA Synthesis Kit (GeneCopoeia).

qPCR primer for microRNA (miR-378a-3p, miR-140-5p, and U6) were purchased from GeneCopoeia. qPCR primer for mRNA (*β-actin, Pparg, Fabp4, Runx2, Alp, Sp7, Bgl, Pparα*) were designed and synthesized by TSINGKE. The primer sequences were listed in Supplemental Table S1. Amplification reactions were performed in 20 μl reaction volume using All-in-One™ miRNA qRT-PCR Detection Kit (GeneCopoeia) and SYBR Green PCR Master Mix (Bio-rad), respectively. U6 was used as a housekeeping gene for miR-378a-3p and miR-140-5p, and β-actin was used for other genes. The cross thresholds (CT) were

normalized to the housekeeping gene, and relative quantification was calculated using ΔΔCT.

2.10. Western blotting

Western blotting was performed as previously described. Primary antibodies for Pparα (ab126285, Abcam) and Abca1 (ab66217, Abcam) were purchased from Abcam. Primary antibody was incubated at 4 °C overnight, and then bound with appropriate secondary antibodies. Blots were visualized using SuperSignal West Pico PLUS Chemiluminescent Substrate.

2.11. Alizarin red S and oil red O assay

Cells were fixed with 4 % neutral paraformaldehyde for 30 min, then washed with PBS thrice. Alizarin red S (Cyagen) and oil red O (Cyagen) staining were conducted according to the manufacturer's introductions.

2.12. Alkaline phosphatase staining

Cells were fixed with 4 % neutral paraformaldehyde for 30 min, then washed with PBS three times. Alkaline Phosphatase (Alp) staining (Solarbio) was performed according to the manufacturer's introductions.

2.13. Micro-CT analyses

We dissected the femurs of mice and fixed them with 4 % neutral paraformaldehyde overnight. The high-resolution μCT was performed to measure bone microstructure. The μCT analyses were performed using high-resolution μCT with a voltage of 65 kV, a current of 153 μA, and a resolution of 15 μm per pixel. The image reconstruction software (NRecon, version 1.6; Bioz) and data analysis software (CTAn v1.9) were used to analyze the parameters of the distal femoral metaphyseal trabecular bone.

2.14. Immunohistochemistry staining

The mice femora were carefully dissected and fixed overnight using 4 % neutral paraformaldehyde. After washing three times with cold PBS, the fixed femurs were decalcified in 10 % EDTA solution for 21 days, and the solution was changed every day. Next, Paraffin embedding after alcohol gradient dehydration. The slides were processed for H&E, Trap staining, and osteocalcin staining. The parameters obtained for the bone formation was osteoblast number per bone perimeter. The parameters obtained for bone marrow fat fraction were adipocyte number per bone marrow surface and proportion of adipocyte area. The parameters measured for bone resorption was osteoclast number per bone perimeter.

2.15. Dual-luciferase reporter gene assay

We constructed the wide type and mutant plasmid of *Pparα* 3′UTR for the predicted binding site of miR-378a at Hanbio Biotechnology Co., Shanghai, China. Next, we transformed the plasmid with Escherichia coli, then coated Luria-Bertani (LB) broth with a bacterial solution to amplify WT-*Pparα*-3′UTR and MUT-*Pparα*-3′UTR. Using Lipofectamine 2000 transfect WT-*Pparα*-3′UTR, MUT-*Pparα*-3′UTR, respectively, and miR-NC mimic or miR-378a mimic for further dual-luciferase reporter gene assay.

2.16. Aptamers conjugation and biodistribution imaging in vivo

We performed aptamer conjugation as previously described [30]. The 5′ end of SSPC aptamer (5′-ACGACGGTGATATGTCAAGG TCGTATGCACGAGTCAGAGG-3′) was engineered with an aldehyde group. Aldehyde-modified SSPC aptamer was designed and constructed by Sangon Biotech, Shanghai, China. 200 nM SSPC aptamer diluent and 1 μg/μl BMM-EVs incubate under constant rotation overnight at 4 °C. The SSPC aptamer conjugated BMM-EVs were washed three times with cold PBS using an Amicon ultrafilter.

One mM near-infrared fluorescent dye DIR (40757ES25, Yeasen) incubated with BMM-EVs and aptamer-conjugated BMM-EVs (BMM-EVs-apt) for 30 min at 4 °C, then washed three times with cold PBS using an Amicon ultrafilter to remove unconjugated DIR. 12 h after tail intravenous injection, the mice were anesthetized and sacrificed.

Fluorescence tomography *in vivo* imaging system was used to capture biodistribution images.

2.17. Statistics

The data were analyzed and mapped using GraphPad Prism 7.0 software.

The student t-test was used for the comparison of two groups and the data was normally distributed, and the approximate *t*-test (Welch's test) was used when the variances of two normally distributed samples were not homogeneous, one-way ANOVA was used for the comparison of three or multiple groups, otherwise, the nonparametric test was used. All experiments were repeated at least three times to guarantee reproducibility of findings, and representative experiments were shown. The experimental data were represented by mean $\pm$ SD, in which $P < 0.05$ indicated the data were statistically different.

3. Results

3.1. Bone marrow macrophage-derived extracellular vesicles from obese mice induce bone deterioration in lean mice

Five-week-old C57BL/6J male mice were fed a high-fat diet (HFD, 60 kcal% energy as fat) or a chow diet for 8 weeks to generate obese and lean mice, respectively. As expected, compared with lean mice, obese mice showed bone deterioration and the propensity of SSPCs to differentiate toward adipocytes (Supplementary Fig. 1). Next, we assessed whether BMMs from obese mice regulate bone deterioration and SSPC function by secreting extracellular vesicles. We isolated BMMs from obese mice (Supplementary Fig. 2, A) and collected BMM-derived extracellular vesicles (BMM-EVs) by ultracentrifugation. Electron microscopy revealed that the BMM-EVs exhibited a "cup shape" (Fig. 1, A), ranging from 90 to 140 nm according to NanoSight analysis (Supplementary Fig. 2, A). Moreover, Western blot analysis revealed that CD9, CD63, and Tsg101 were enriched in BMM-EVs compared with parental cells and that the endoplasmic reticulum-specific integral protein calnexin was barely detected in BMM-EVs (Fig. 1, A). These data indicate that BMM-EVs were successfully isolated. Then, using lean mice as recipients, we injected BMM-EVs from lean mice (lean BMM-EVs) and BMMs-EVs from obese mice (obese BMM-EVs) (100 μg twice a week) into recipient mice via the tail vein for two months to investigate whether obese BMM-EVs contribute to obesity-related bone deterioration (Fig. 1, B). First, we found that body weight was comparable between the two groups (Supplementary Fig. 2, B). Moreover, micro-CT analysis revealed that compared with those in the lean BMM-EV-treated group, the trabecular bone mass in the obese BMM-EV-treated group was lower (Fig. 1, C-G and Supplementary Fig. 2, C and D).
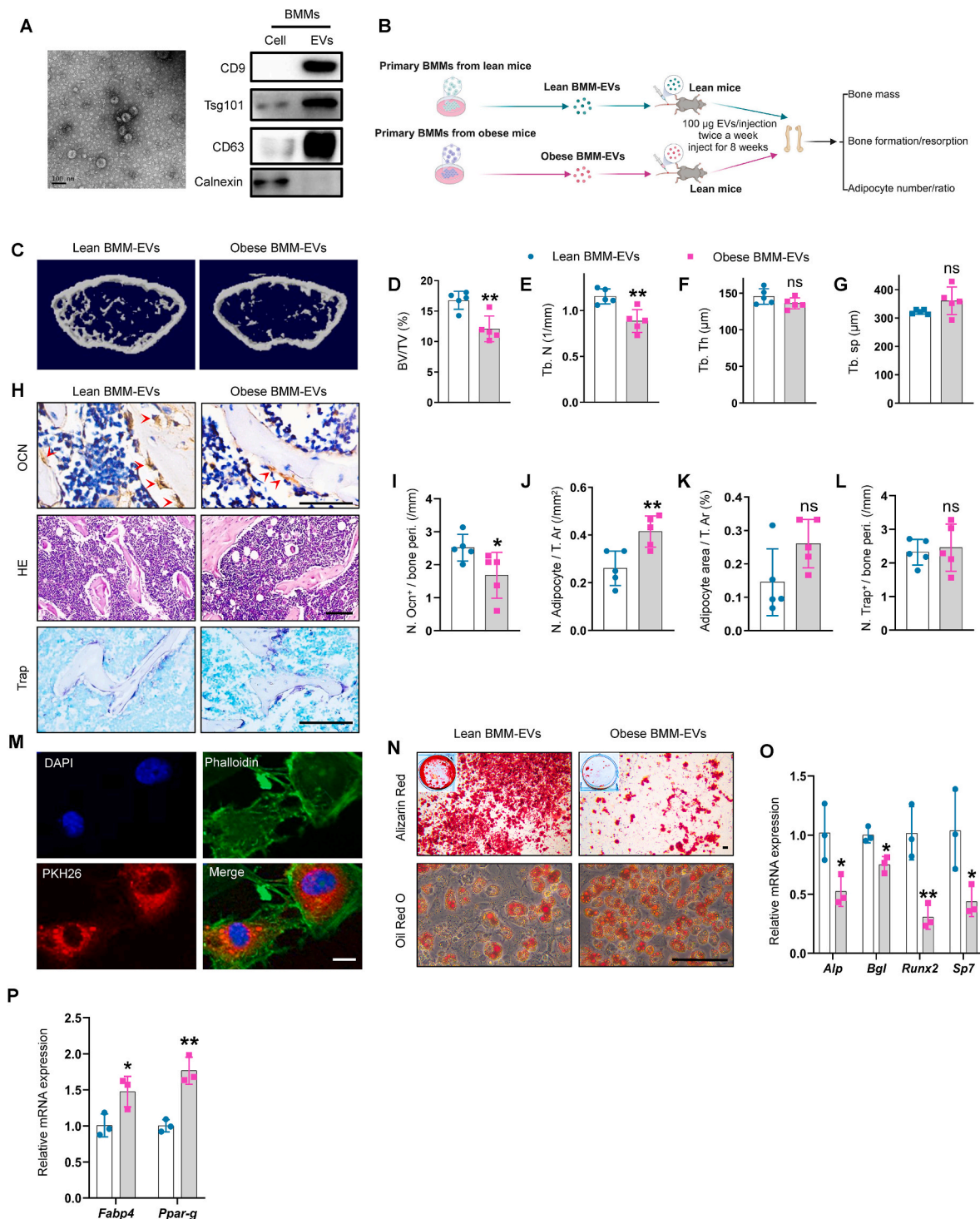
Fig. 1. Bone marrow macrophage-derived extracellular vesicles from obese mice induce bone deterioration in lean mice.
(A) Representative picture of BMM-EVs (left), scale bar: 100 nm; representative western blotting images of CD9, Tsg101, CD63, and Calnexin in cell lysis of bone marrow macrophage and BMM-EVs (right). (B) Schematic diagram of lean mice with lean/obese BMM-EVs intervention. (C) Representative μCT images of lean mice with lean/obese BMM-EVs intervention. n = 5 per group. (D–G) Quantitative μCT analysis of BV/TV, Tb. N, Tb. Th, and Tb. Sp from lean mice with lean/obese BMM-EV intervention. n = 5 per group. (H) Representative images of osteocalcin immunohistochemical staining (H, top). Red arrows mark osteoblasts. Scale bar: 50 μm; representative images of H&E staining (H, middle), and Trap staining (H, bottom) in distal femora. Scale bar: 100 μm. (I–K) Quantification of the number of osteocalcin-positive osteoblasts (I) and number and area of adipocytes (J–K). (L) Quantification of osteoclast number in distal femora from lean mice with lean/obese BMM-EV intervention. (M) BMM-EVs were taken up by SSPCs. Red fluorescence represents PKH26 marked extracellular vesicles; green fluorescence represents phalloidin labeled cytoskeleton, and blue fluorescence indicates nuclei. Scale bar: 2.5 μm. (N) Representative images of Alizarin red staining of lean BMM-EV and obese BMM-EV-treated SSPCs (N, top); representative images of oil red O staining of lean BMM-EV and obese BMM-EV-treated SSPCs (N, bottom). n = 3 per group. Scale bar: 100 μm. (O–P) qRT-PCR analysis of the relative expression levels of osteogenic genes (O) and adipogenic genes (P) in lean BMM-EV and obese BMM-EV-treated SSPCs cultured in osteogenesis and/or adipogenesis induction medium. Data is shown as mean ± SD. *$P < 0.05$, **$P < 0.01$, ns, no significant. (Welch's test is used in Fig. 1G, and student t-test is used in others).

Immunohistochemical staining analysis revealed that compared with lean BMM-EV-treated control mice, obese BMM-EV-treated mice had fewer osteocalcin-positive osteoblasts on the trabecular bone surface and a greater number of adipocytes in the bone marrow (Fig. 1, H–K). There was no significant difference in the number of osteoclasts on the bone surface between obese BMM-EV-treated mice and lean BMM-EV-treated control mice (Fig. 1, H and L). Additionally, because BMM-EVs are secreted by macrophages (vital immune cells), we investigated whether lean and obese BMM-EVs trigger different degrees of inflammatory reactions in recipient mice. Enzyme Linked Immunosorbent Assay (ELISA) revealed that the levels of the proinflammatory factors IL-6 and IL-1α did not significantly differ between the serum of lean and obese BMM-EV-treated mice (Supplementary Fig. 2, E-F).

Next, we tested the hypothesis that obese BMM-EVs regulate SSPC fate switching between osteoblasts and adipocytes *in vitro*. The uptake of PKH26-labeled BMM-EVs by SSPCs was characterized by the appearance of red fluorescent PKH26 dye in SSPCs (Fig. 1, M). Compared with the administration of lean BMM-EVs, the administration of obese BMM-EVs inhibited SSPC osteogenic differentiation and mineralization, as evidenced by the decreased expression of osteogenic-related genes (*Alp*, *Runx2*, *Bgl*, and *Sp7*) and fewer calcium nodules, as measured by Alizarin red staining (Fig. 1, O and N). Compared with those in the control group, SSPCs treated with obese BMM-EVs showed enhanced adipogenic differentiation, as indicated by the increased expression of adipogenic-related genes (*Fabp4* and *Ppar-g*) and increased lipid droplet density, as measured by qPCR analysis and oil red O staining, respectively (Fig. 1,
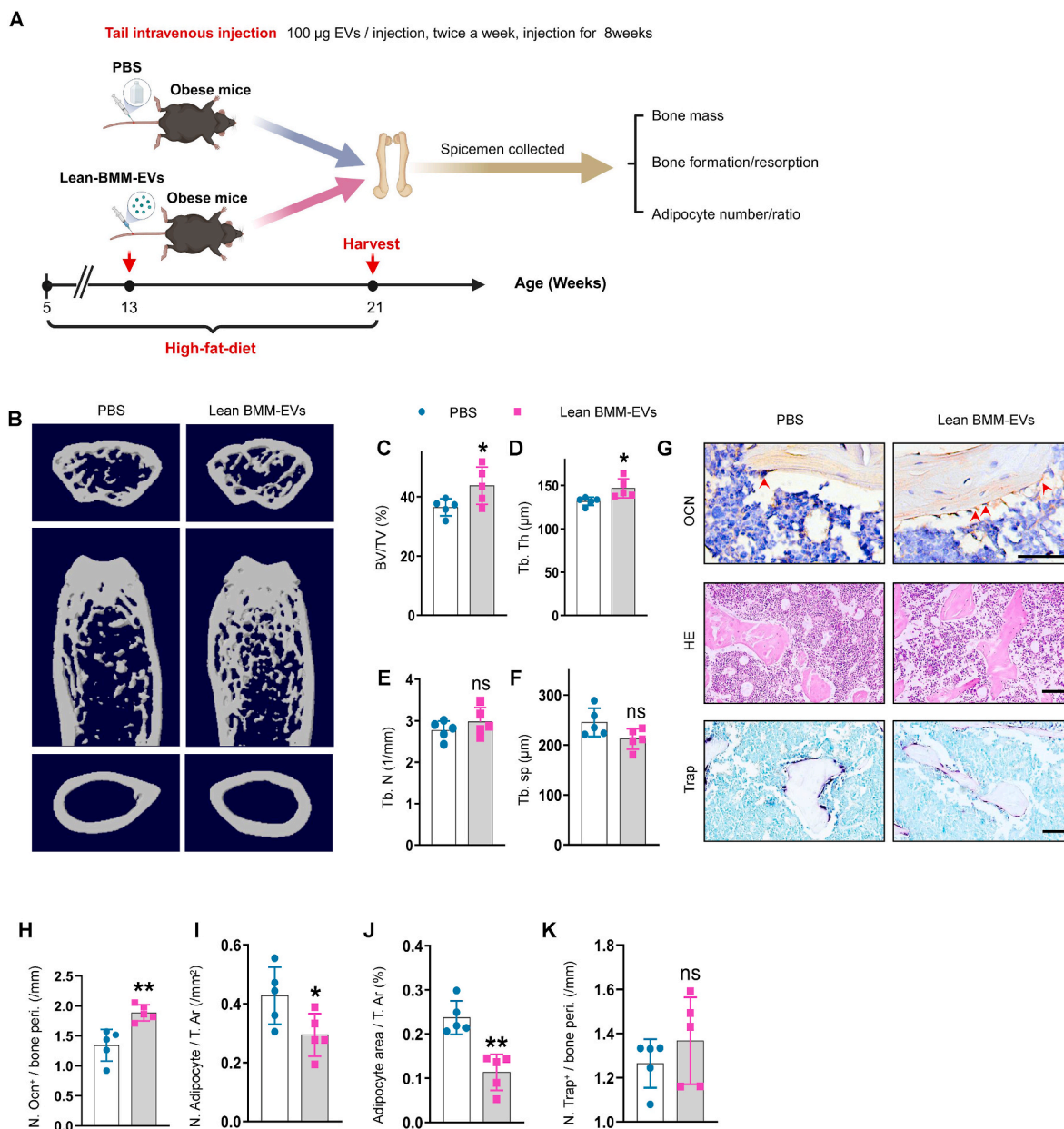
Fig. 2. Lean BMM-EVs ameliorate bone deterioration and marrow fat accumulation in obese mice.
5-week-old C57BL/6J male mice were fed with a high-fat diet for 2 months, then treated these obese recipient mice with lean BMM-EVs for 2 months (100 μg, twice a week) and collected distal femora for further study. (A) Schematic diagram of obese mice with PBS and lean BMM-EV intervention. (B-F) Representative μCT images (B) and quantitative μCT analysis of trabecular bone (C-F) from obese mice with PBS and/or lean BMM-EV intervention. n = 5 per group. (G) Representative images of osteocalcin immunohistochemical staining (G, top). Red arrows mark osteoblasts. Scale bar: 50 μm; representative images of H&E staining (G, middle) and Trap staining (G, bottom) in distal femora. Scale bar: 100 μm. (H-K) Quantification of the number of osteoblasts (H); number and area of adipocytes (I-J) and number of Trap-positive osteoclasts (K). Data is shown as mean ± SD. *$P < 0.05$, **$P < 0.01$, ns, no significant. (Student *t*-test).

P and N). Together, these data indicate that obese BMM-EVs promote bone deterioration, suppress osteogenesis, and promote the adipogenesis of SSPCs.

3.2. Lean BMM-EVs ameliorate bone deterioration and marrow fat accumulation in obese mice

Given the negative impacts of obese BMM-EVs on bone homeostasis, we next evaluated whether lean BMM-EVs could mitigate bone deterioration in obese mice (Fig. 2, A). Two months of treatment of obese recipient mice with lean BMM-EVs (100 μg, twice a week) led to increased trabecular bone mass (Fig. 2, B-F), with no significant difference in cortical bone thickness or body weight (Supplementary Fig. 2, G and H). Immunohistochemicalstaining analysis revealed that obese recipient mice administered lean BMM-EVs had a greater number of osteoblasts on the trabecular bone surface (Fig. 2, G and H) and less adipocyte accumulation in the bone marrow compared to those in the control group (Fig. 2, G and I-J). Treatment with lean BMM-EVs did not affect the number of osteoclasts on the trabecular bone surface (Fig. 2, G and K). Taken together, these results suggest that BMM-EVs produced in the lean state protect against obesity-induced bone deterioration and marrow fat accumulation.

3.3. BMM-EV microRNA-378a-3p and microRNA-140-5p may coordinately regulate SSPC lineage fate

To assess obesity-induced changes in the microRNA profile of BMM-EVs, we performed a miRNA array analysis of obese and lean BMM-EVs. A total of 1888 differentially expressed microRNAs were identified in obese BMM-EVs versus lean BMM-EVs. We comprehensively evaluated basal expression, significant differences, fold changes, sequence conservation, and novelty and selected six microRNAs—three upregulated microRNAs (microRNA-1839-5p, microRNA-221-5p, and microRNA-140-5p) and three downregulated microRNAs (microRNA-378a-3p, microRNA-378c, and microRNA-378d)—for further study (Fig. 3, A). The effects of these six microRNAs on SSPC osteogenic and adipogenic differentiation were investigated *in vitro*. qPCR analysis revealed that among the three upregulated microRNAs, microRNA-140-5p (hereafter, miR-140) inhibited the expression of osteogenesis-related genes (*Alp* and *Sp7*) and promoted the expression of adipogenesis-related genes (*Fabp4*) (Fig. 3, B and Supplementary Fig. 3, A-C). Among the three downregulated microRNAs, microRNA-378a-3p (hereafter, miR-378a) promoted the expression of osteogenesis-related genes (*Alp* and *Sp7*) and suppressed the expression of adipogenesis-related genes (*Fabp4* and *Ppar-g*) (Fig. 3, C and Supplementary Fig. 3, D-F). Combined with the increased miR-140 and decreased miR-378 levels in obese BMM-EVs (Fig. 3, A and Supplementary Fig. 3, G and H), we speculate that BMM-EV miR-378a and miR-140 may coordinately regulate SSPC lineage fate in obese mice. Thus, we selected miR-140 and miR-378a for subsequent analyses. Alizarin red and oil red O staining analysis revealed that miR-140 suppressed SSPC osteogenic differentiation and mineralization and promoted lipid droplet formation, and miR-378a enhanced osteogenesis and inhibited adipogenesis (Fig. 3, D and E). Furthermore, to determine whether miR-140 or miR-378a encapsulated in BMM-EVs could regulate the SSPC lineage fate of osteogenic and adipogenic commitment, we transfected miR-140 or miR-378a into macrophages and collected miR-140- and miR-378a-enriched macrophage-derived extracellular vesicles. We found that SSPCs treated with miR-140-enriched BMM-EVs exhibited enhanced adipogenesis but impaired osteogenic potential (Fig. 3, F and G) and that miR-378a-enriched BMM-EVs promoted SSPC osteogenic differentiation and inhibited adipogenic differentiation (Fig. 3, H and I). These results suggest that miR-378a promotes SPPC differentiation into osteoblasts rather than into adipocytes, miR-140 predisposes SSPCs to differentiate into adipocytes, and decreased miR-378a and increased miR-140 levels in BMM-EVs may coordinately regulate SSPC osteogenic and adipogenic

differentiation.

### 3.4. Conditional miR-140 knockout in BMMs mitigate bone deterioration in obese mice

Given that the level of miR-140 was greater in obese BMM-EVs and promoted SSPC adipogenesis *in vitro*, we wondered whether the depletion of miR-140 in BMMs could reverse bone deterioration and marrow fat accumulation in obese mice. To generate a mouse model with conditional depletion of miR-140 in BMMs, we constructed miR-140$^{flox/flox}$ mice and fed 5-week-old miR-140$^{flox/flox}$ mice a high-fat diet for 2 months. Then, these obese miR-140$^{flox/flox}$ mice received intra-bone marrow injections of an adeno-associated virus containing the F4/80 promoter followed by the Cre and ZsGreen sequences (AAV-F4/80-Cre-ZsGreen and fed with a high-fat diet for 2 months to generate an obese mouse model with conditional miR-140 depletion in BMMs (miR-140$^{BMMs\triangle}$) (Fig. 4, A). miR-140$^{flox/flox}$ mice treated with AAV-NC-ZsGreen were used as controls (miR-140$^{BMMs+/+}$). The co-staining of ZsGreen fluorescence and F4/80-positive red fluorescence in femur sections indicated successful AAV transfection in BMMs (Supplementary Fig. 4, A). Next, we analyzed the bone phenotype of miR-140$^{BMM\triangle}$ mice. Micro-CT analysis revealed greater trabecular bone volume and trabecular bone number and less trabecular bone separation in the femurs of miR-140$^{BMMs\triangle}$ mice compared with those in the femurs of miR-140$^{BMMs+/+}$ mice (Fig. 4, B-C and Supplementary Fig. 4, B-F). In addition, miR-140$^{BMMs\triangle}$ mice had a greater number of osteoblasts on the trabecular bone surface and a lower number and area of adipocytes in the bone marrow (Fig. 4, D-F and Supplementary Fig. 4, G). These data indicate that BMM-derived miR-140 may have negative effects on bone and that the depletion of miR-140 in BMMs may mitigate bone deterioration and marrow fat accumulation in obese mice.

3.5. Mice with SSPC miR-140 conditional overexpression exhibit decreased bone mass and bone marrow fat accumulation

The above data indicate that BMM-derived miR-140 may regulate SSPC osteoblastic and adipogenic differentiation. To further test the direct effect of miR-140 on SSPCs, we generated SSPCs miR-140-overexpressing mice (miR-140$^{SSPC-OE}$) by crossing miR-140 TG$^{flox/flox}$ mice with Prrx1-cre mice (Fig. 4, G). We collected femurs from miR-140$^{SSPC-OE}$ and miR-140 TG$^{flox/flox}$ mice for micro-CT analysis and bone section staining. Compared with miR-140 TG$^{flox/flox}$ mice, miR-140$^{SSPC-OE}$ mice exhibited lower trabecular bone volume, trabecular bone number, and cortical bone thickness (Fig. 4, H–I, Supplementary Fig. 4, H-L). In addition, immunohistochemical staining revealed greater bone marrow fat accumulation in miR-140$^{SSPC-OE}$ mice than in control mice (Fig. 4, J-N). These results suggest that the conditional overexpression of miR-140 induces a switch in SSPC differentiation toward adipocytes, which leads to decreased bone mass and marrow fat accumulation in lean mice.

3.6. Lean mice with BMMs conditional miR-378a depletion exhibit low bone mass and marrow fat accumulation

After verifying the effects of BMM-derived miR-140 on obesity-induced bone deterioration, we investigated the effect of another selected microRNA, miR-378a, which promotes osteogenesis *in vitro*, on bone *in vivo*. Using the same strategy, we constructed miR-378a$^{flox/flox}$ mice, which then received intramedullary injections of AAV-F4/80-Cre-ZsGreen to generate a mouse model with conditional depletion of miR-378a in BMMs (miR-378a$^{BMMs\triangle}$) (Fig. 5, A and Supplementary Fig. 5, A). miR-378a$^{flox/flox}$ mice treated with AAV-NC-ZsGreen were used as controls (miR-378a$^{BMMs+/+}$). We conducted micro-CT analysis to evaluate the bone microstructure and observed less trabecular bone mass and greater trabecular bone separation in the femurs of miR-378a$^{BMMs\triangle}$ mice than in the femurs of miR-378a$^{BMMs+/+}$ mice (Fig. 5, B-
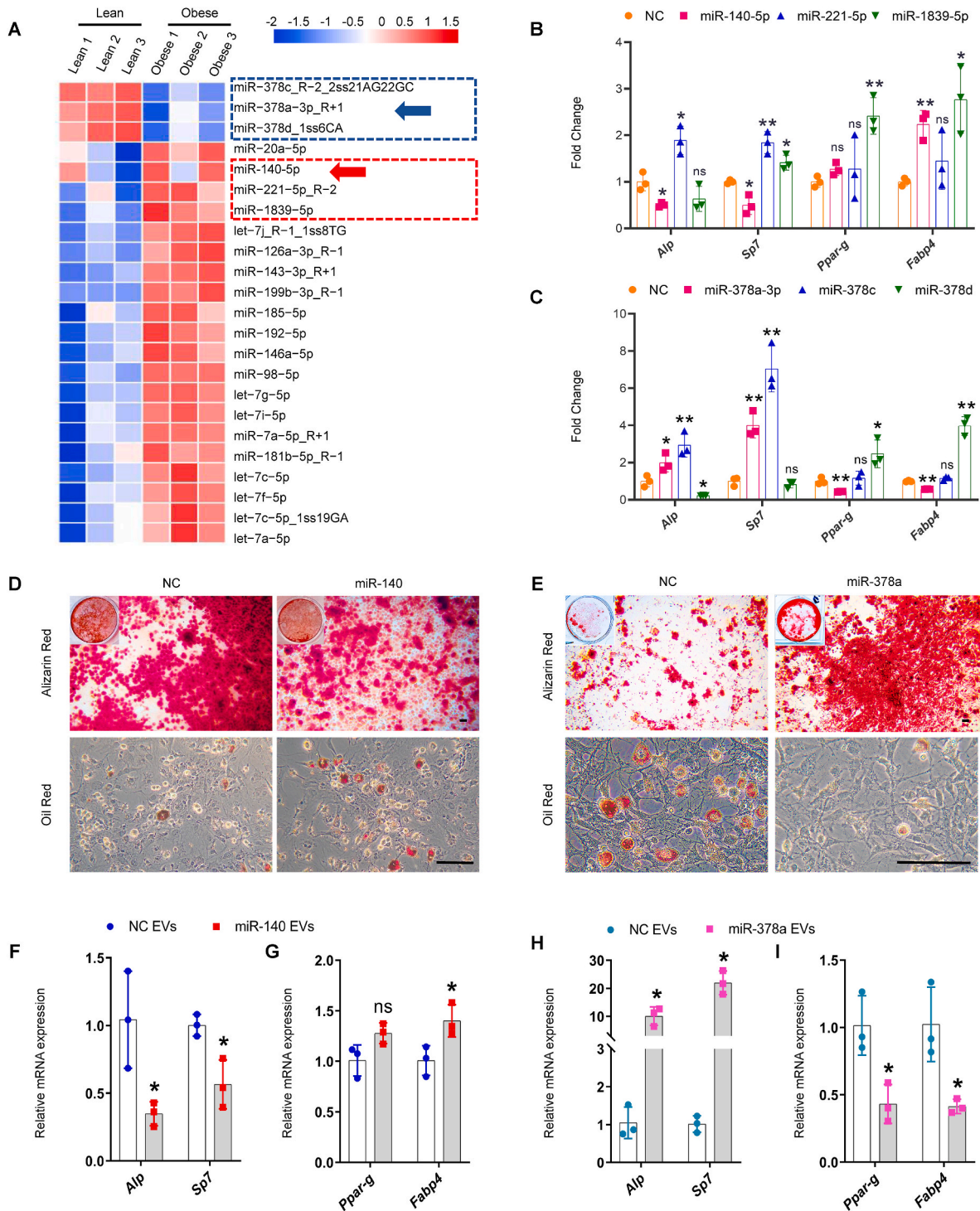
Fig. 3. BMM-EV miR-378a-3p and miR-140-5p may coordinately regulate SSPC lineage fate.

(A) miRNA microarray analyzes the differently expressed microRNAs in lean BMM-EVs and obese BMM-EVs. The red rectangle circles three up-regulated microRNAs in obese BMM-EVs, and the blue rectangle circles three down-regulated microRNAs. The arrows mark the microRNAs chosen for further functional verification. n = 3 per group. (B) qRT-PCR analysis of the relative expression levels of osteogenic genes (*Alp, Sp7*) and adipogenic genes (*Ppar-g, Fabp4*) of the SSPCs transfected with three up-regulated microRNAs (miR-140-5p, miR-221-5p, and miR-1839-5p) and their negative controls, which culture in osteogenic and adipogenic medium for 6 days, respectively. NC, negative control. n = 3 per group. (C) qRT-PCR analysis of the relative expression levels of osteogenic genes (*Alp, Sp7*) and adipogenic genes (*Ppar-g, Fabp4*) of the SSPCs transfected with three downregulated microRNAs (miR-378a-3p, miR-378c, and miR-378d) and their negative controls for 6 days, respectively. n = 3 per group. (D) Representative images of Alizarin red staining (D, top) and oil red O staining (D, bottom) of the SSPCs transfected with miR-140 and negative controls. Scale bar: 100 μm. (E) Representative images of Alizarin red staining (E, top) and oil red O staining (E, bottom) of the SSPCs transfected with miR-378a and negative controls. Scale bar: 100 μm. (F-I) BMM-EVs overloaded with miR-140 and miR-378a regulate SSPC lineage fate between osteoblasts and adipocytes. qRT-PCR analysis of the relative expression levels of osteogenic genes (F and H) and adipogenic genes (G and I) in miRNA-140 enriched macrophage-derived extracellular vesicle and miR-378a enriched macrophage-derived extracellular vesicle-treated SSPCs. n = 3 per group. Data is shown as mean ± SD. *$P <$ 0.05, **$P < 0.01$, ns, no significant. (Welch's test is used in the *Fabp4* expression of Fig. 3B, *Ppar-g* and *Fabp4* expression of Fig. 3C, *and* Alp, Sp7 expression in Fig. 3H, non-parametric test is used in Sp7 expression of Fig. 3C and student *t*-test is used in others).
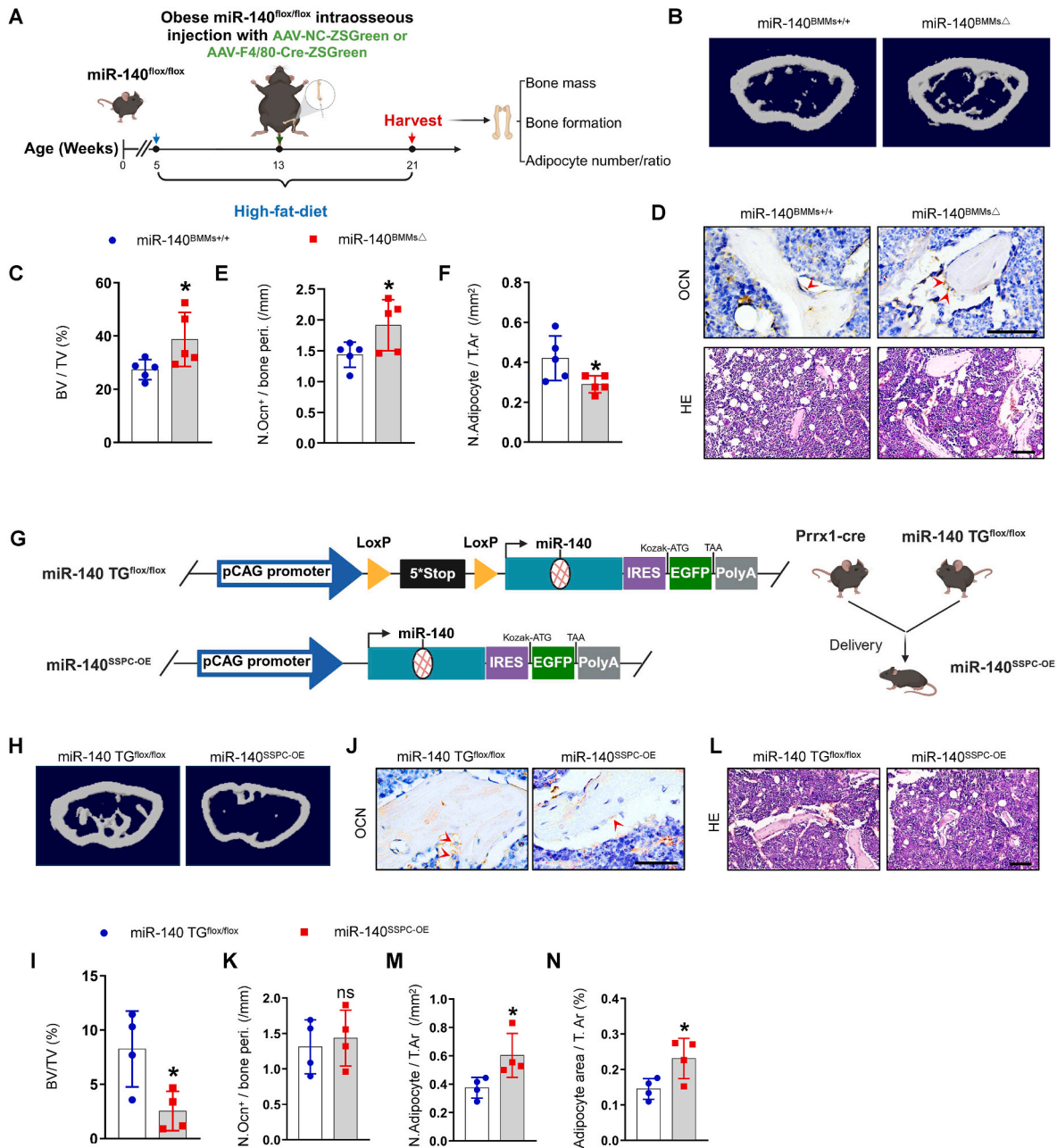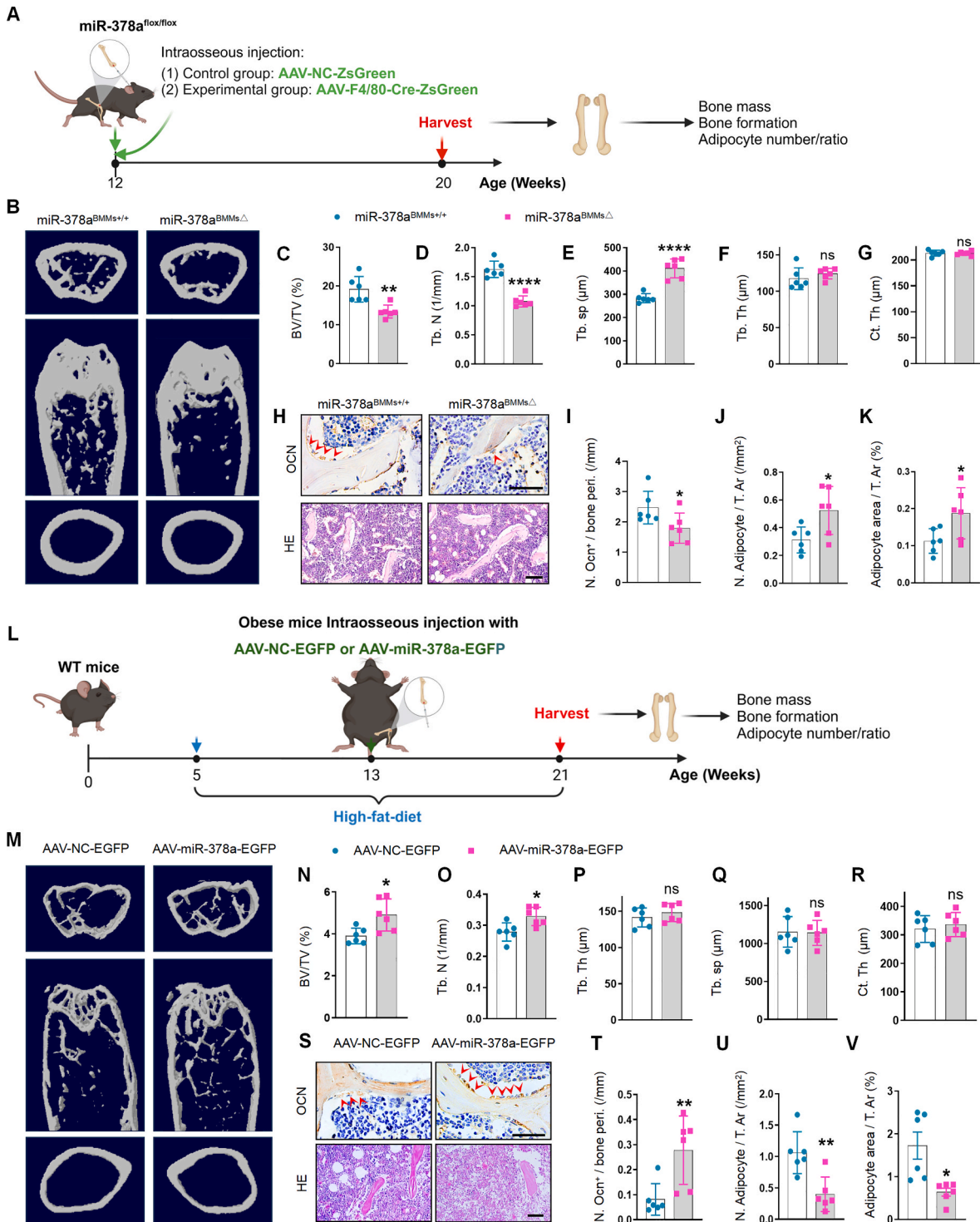
Fig. 4. Conditional miR-140 knockout and conditional miR-140 over-expression regulate bone deterioration and SSPC cell fate *in vivo*.
(A-F) Adeno-associated-virus-F4/80-cre-ZsGreen (AAV-F4/80-Cre-ZsGreen) and adeno-associated-virus-NC-ZsGreen (AAV-NC-ZsGreen) were injected into intra bone marrow of obese miRNA-140$^{flox/flox}$ littermate to generate BMM conditional miRNA-140 knockout mice and negative controls. Two months after injection, femur specimens were collected. n = 5 per group. (A) Timeline diagram of obese BMM conditional miRNA-140 knockout mice generation. (B–C) Representative μCT images (B) and quantitative μCT analysis (C) of trabecular bone. (D) Representative images of osteocalcin staining (D, top). Red arrows mark osteoblasts. Scale bar: 50 μm; representative images of H&E staining (D, bottom). Scale bar: 100 μm; (E-F) Quantification of the number of osteoblasts (E) and number of adipocytes (F). (G–N) Cross miRNA-140TG$^{flox/flox}$ mice with Prrx1-cre mice to generate SSPC conditional miR-140 over-expression mice (miRNA-140$^{SSPC-OE}$). (G) Diagram of miR-140TG$^{flox/flox}$ mice construct and miRNA-140$^{SSPC-OE}$ mice generation. An exogenous donor sequence containing terminators and miR-140 was inserted into chromosome 11 in wild-type mice. Loxp sites are depicted by yellow arrows, miR-140$^{SSPC-OE}$ represents Prrx1-cre; miR-140TG$^{flox/+}$ mice. (H-I) Representative μCT images (H) and quantitative μCT analysis of trabecular bone (I) from miRNA-140$^{SSPC-OE}$ and miRNA-140 TG$^{flox/flox}$ mice. n = 4 per group. (J–K) Representative images of osteocalcin staining (J) and quantification of number of osteoblasts (K). n = 4 per group. Red arrows mark osteoblasts. Scale bar: 50 μm. (L-N) Representative images of H&E staining (L) and number and area of adipocytes (M-N). Scale bar: 100 μm. Data is shown as mean ± SD. *$P < 0.05$, **$P < 0.05$, ns, no significant. (Student *t*-test).

G). Immunohistochemical staining revealed fewer osteocalcin-positive osteoblasts on the bone surface and more adipocytes in the bone marrow of miR-378a$^{BMMs△}$ mice than in the bone marrow of control mice (Fig. 5, H-K). These results indicate that BMM-derived miR-378a promotes osteoblastic bone formation and inhibits marrow fat accumulation and that the depletion of miR-378a in BMMs leads to low bone mass and marrow fat accumulation, similar to obesity-induced bone deterioration.

3.7. miR-378a overexpression increases bone mass in obese mice

The above data prompted us to test the therapeutic effect of miR-

Fig. 5. Conditional miR-378a knockout and miR-378a over-expression modulate bone mass and marrow fat accumulation.
(A-K) AAV-F4/80-Cre-ZsGreen and AAV-NC-ZsGreen were injected into the bone cavity of miRNA-378a^flox/flox^ littermate to generate BMM conditional miRNA-378a knockout mice (miRNA-378a^BMMsΔ^) and their controls. 2 months after injection, the mice are sacrificed. n = 6 per group. (A) Timeline diagram of BMM conditional miR-378a knockout mice generation. (B-G) Representative μCT images (B) and quantitative μCT analysis of trabecular (C-F) and cortical bone (G) from lean miR-378a^BMMsΔ^ and miRNA-378a^BMMs+/+^ mice. (H) Representative images of osteocalcin staining (H, top). Red arrows mark osteoblasts. Scale bar: 50 μm; representative images of H&E staining (H, bottom). Scale bar: 100 μm. (I-K) Quantification of number of osteoblasts (I) and number and area of adipocytes (J-K). (L-V) Adeno-associated-virus-miR-378a-EGFP (AAV-miR-378a-EGFP) and adeno-associated-virus-NC-GFP (AAV-NC-EGFP) were injected into the bone cavity in obese mice with the same age and gender. 2 months after injection, the mice are sacrificed. (L) Timeline diagram of miR-378a-overexpressing mice generation. (M) Representative μCT images of AAV-miR-378a-EGFP and AAV-NC-EGFP treated mice. n = 6 per group. (N-Q) Quantitative μCT analysis of trabecular bone. (R) Quantitative μCT analysis of cortical bone. (S) Representative images of osteocalcin staining (S, top). Red arrows mark osteoblasts. Scale bar: 50 μm; representative images of H&E staining (S, bottom). Scale bar: 100 μm. (T-V) Quantification of the number of osteoblasts (T) and number and area of adipocytes (U-V) in distal femora. Data is shown as mean ± SD. *P < 0.05, **P < 0.01, ****P < 0.0001, ns, no significant. (Non-parametric test is used in Fig. 5 I and Fig. 5 T, Welch's test is used in Fig. 5 V, student *t*-test is used in others).

378a on obesity-induced bone deterioration *in vivo*. We constructed an adeno-associated virus, pAAV-CMV-EGFP-3xFLAG-miR-378a-3p-WPRE (AAV-miR-378a-3p-EGFP), to overexpress miR-378a in bone tissue through the intramedullary injection of AAV-miR-378a-3p-EGFP (25 μl, 3.2*10^12 vg/ml) in obese mice (Fig. 5, L). Eight weeks after injection, we collected the femurs and analyzed the bone phenotype. The appearance of green fluorescence in femur sections and the increased level of miR-378a in femur tissue indicated that AAV-miR-378a-3p-

EGFP was successfully transfected into the femur (Supplementary Fig. 5, B and C). Furthermore, mice treated with AAV-miR-378a-3p-EGFP showed significantly greater trabecular bone volume and trabecular bone number than vehicle-treated mice (Fig. 5, M–R). Moreover, the administration of AAV-miR-378a-3p-EGFP increased the number of osteoblasts on the trabecular bone surface and decreased the number and area of lipid droplets in the bone marrow of obese mice (Fig. 5, S–V). These results indicated that miR-378a treatment alleviated bone
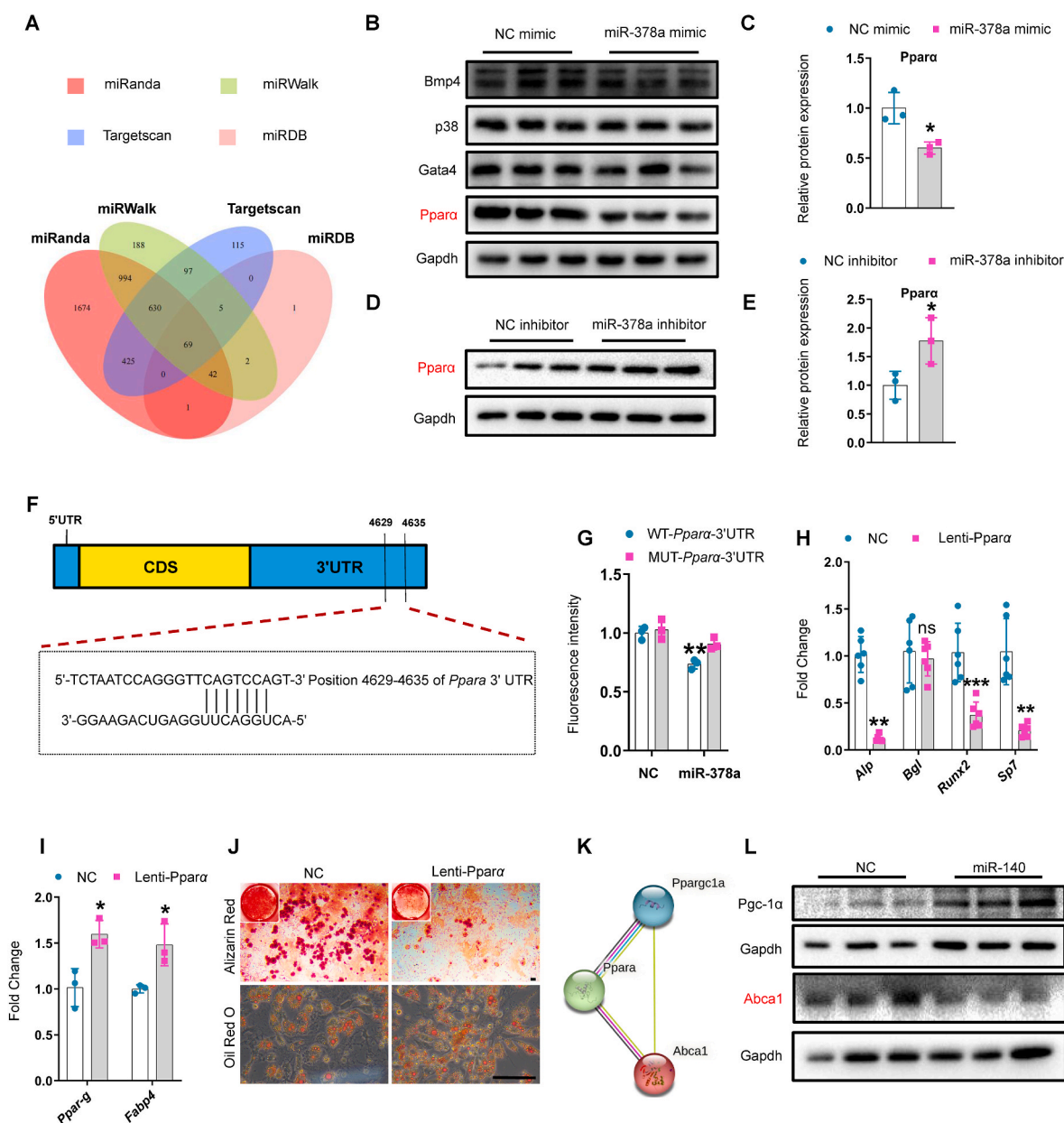

Fig. 6. miR-378a and miR-140 synergistically regulated SSPC lineage fate via targeting the Pparα-Abca1 axis.
(A) Venn diagram of the miR-378a target gene. (B-C) Representative western blotting images of Bmp4, p38, Gata 4, Pparα, and Gapdh (B); quantification of Pparα expression (C) in SSPCs transfected with the mimic of miR-378a and its negative controls for 3 days. n = 3 per group. (D-E) Representative western blotting images of Pparα (D) and quantification of Pparα expression (E) in SSPCs transfected with the inhibitor of miR-378a and its negative controls for 3 days. n = 3 per group. (F) Schematic of miR-378a putative target sites in mouse *Pparα* 3′-UTR. CDS, coding sequence. (G) SSPCs were transfected with luciferase reporter carrying WT or MUT 3′-UTR of the *Pparα* gene (WT-*Pparα*-Fluc and/or Mut-*Pparα*-Fluc) and co-transfected with miR-NC and/or miR-378a, respectively. Fluorescence intensity was determined at 48 h after transfection; the asterisk means WT-*Pparα*-3′-UTR co-transfected with miR-NC *vs.* WT-*Pparα*-3′-UTR co-transfected with miR-378a (H-I) SSPCs were transfected with lenti-Pparα to induce osteogenesis and/or adipogenesis for 6 days. qRT-PCR analysis of the relative expression levels of osteogenic genes (H), n = 6 per group, and adipogenic genes (I), n = 3 per group. (J) Representative images of Alizarin red staining (J, top) and oil red O staining (J, bottom). Scale bar: 100 μm, n = 3 per group. (K) Schematic of protein interaction diagram of Pparα, Abca1, and Pgc-1α. (L) Representative western blotting images of Abca1 and Pgc-1 in SSPCs transfected with miR-140 and its negative controls. n = 3 per group. Data is shown as mean ± SD. *P < 0.05, **P < 0.01, ***P < 0.001, ns, no significant. (Non-parametric test is used in *Alp* expression of Fig. 6H, Welch's test is used in *Sp7* expression of Fig. 6H, and student *t*-test is used in others).

deterioration in obese mice.

3.8. miR-378a and miR-140 synergistically regulate SSPC lineage fate by targeting the Pparα-Abca1 axis

Based on the above data, we hypothesized that miR-378a and miR-140 synergistically influence SSPC lineage fate. We used several target prediction tools, including TargetScan, miRanda, miRDB, and miRWalk, to predict target genes of miR-378a based on the complementary base pairing principle. Sixty-nine overlapping target genes of miR-378a were predicted by all four-target prediction tools (Fig. 6, A). We selected several genes associated with osteogenesis and adipogenesis, including Pparα, Gata4, p38, and Bmp4, for further verification. SSPCs transfected with a miR-378a mimic showed reduced protein levels of Pparα but no changes in the protein levels of GATA4, p38, or BMP4 (Fig. 6, B and C). In addition, the protein level of Pparα was significantly greater in SSPCs transfected with the miR-378a inhibitor than in those transfected with the control (Fig. 6, D and E). In contrast, the mRNA expression level of *Pparα* was unaffected, indicating that miR-378a post-transcriptionally regulates *Pparα* (Supplementary Fig. 6, A and B). According to the base complementary pairing principle, miR-378a may target bases 4629-4635 of the *Pparα* 3′-UTR (Fig. 6, F). We constructed a *Pparα* plasmid containing the predicted binding site (WT-*Pparα*-Fluc) of miR-378a and a mutant *Pparα* plasmid containing a mutation in the predicted binding site (Mut-*Pparα*-Fluc). Luciferase reporter assay results indicated that miR-378a inhibited the luciferase activity of the WT-*Pparα*-Fluc reporter genes and that Mut-*Pparα*-Fluc eliminated the repressive effect of miR-378a, confirming the direct binding of miR-378a to the 3′-UTR of *Pparα* (Fig. 6, G). Furthermore, the use of Pparα-overexpressing lentiviruses (Lenti-Pparα) to overexpress *Pparα* in SSPCs resulted in the inhibition of SSPC osteoblastic differentiation and promoted adipogenic differentiation (Fig. 6, H-J and Supplementary Fig. 6, C-D). These results suggest that miR-378a may regulate the SSPC lineage fate of osteoblasts and adipocytes by targeting Pparα.

Given the synergistic regulatory effect of miR-378a and miR-140 on SSPC lineage fate, we tested whether miR-140 could directly target Pparα. The transfection of miR-140 did not affect the protein level of Pparα (Supplementary Fig. 6, E); therefore, we assumed that miR-140 may regulate target gene/genes that can interact with Pparα. We used TargetScan and the protein-protein interaction (PPI) network database STRING to analyze miR-140-targeted genes involved in Pparα signaling pathways. Among the candidates, Ppargc-1α (Pgc-1α) and Abca1, which have been reported to be involved in regulating osteogenesis and adipogenesis, were further studied (Supplementary Fig. 6, F and Fig. 6, K). The transfection of miR-140 reduced the protein level of Abca1, but not that of Pgc-1α, in SSPCs compared to the control (Fig. 6, L). Abca1 is reportedly a positive regulator of osteogenesis [36] and a downstream molecule of the Pparα signaling pathway and is negatively regulated by Pparα [37]. Together, our data indicate that miR-140 may inhibit osteogenesis by targeting the Pparα signaling pathway downstream molecule Abca1. These results suggested that miR-378a and miR-140 may synergistically regulate SSPC lineage fate by directly targeting the Pparα-Abca1 axis. To further test whether miR-378a and miR-140 synergistically influence SSPC lineage fate, we co-transfected a miR-378a mimic and miR-140 inhibitor into SSPCs and subjected the resulting SSPCs to osteogenic induction. qRT-PCR analysis exhibits higher Alp expression in SSPCs treated with microRNA-378a-3p mimics plus microRNA-140-5p inhibitors than those treated with microRNA-378a-3p mimics or microRNA-140-5p inhibitors alone, but the expression of Runx2 is no significant difference between SSPCs treated with microRNA-378a-3p mimics plus microRNA-140-5p inhibitors and those treated with microRNA-378a-3p mimics or microRNA-140-5p inhibitors alone. Also, the expression of Bgl and Sp7 is no significant difference between SSPCs treated with microRNA-378a-3p mimics plus microRNA-140-5p inhibitors and those treated with microRNA-378a-3p mimics alone (Supplementary Fig. 6,

G). In addition, alkaline phosphatase (Alp) staining also suggested that the co-transfection of microRNA-378a-3p mimics and microRNA-140-5p inhibitors didn't predominantly amplify the osteogenic effect than those transfected microRNA-378a-3p mimics alone (Supplementary Fig. 6, H), this can be explained by that microRNA-378a-3p and microRNA-140-5p regulate SSPC differentiation through the same pathway. Together, these data indicated that miR-378a and miR-140 synergistically regulate SSPC lineage fate by targeting the Pparα-Abca1 axis.
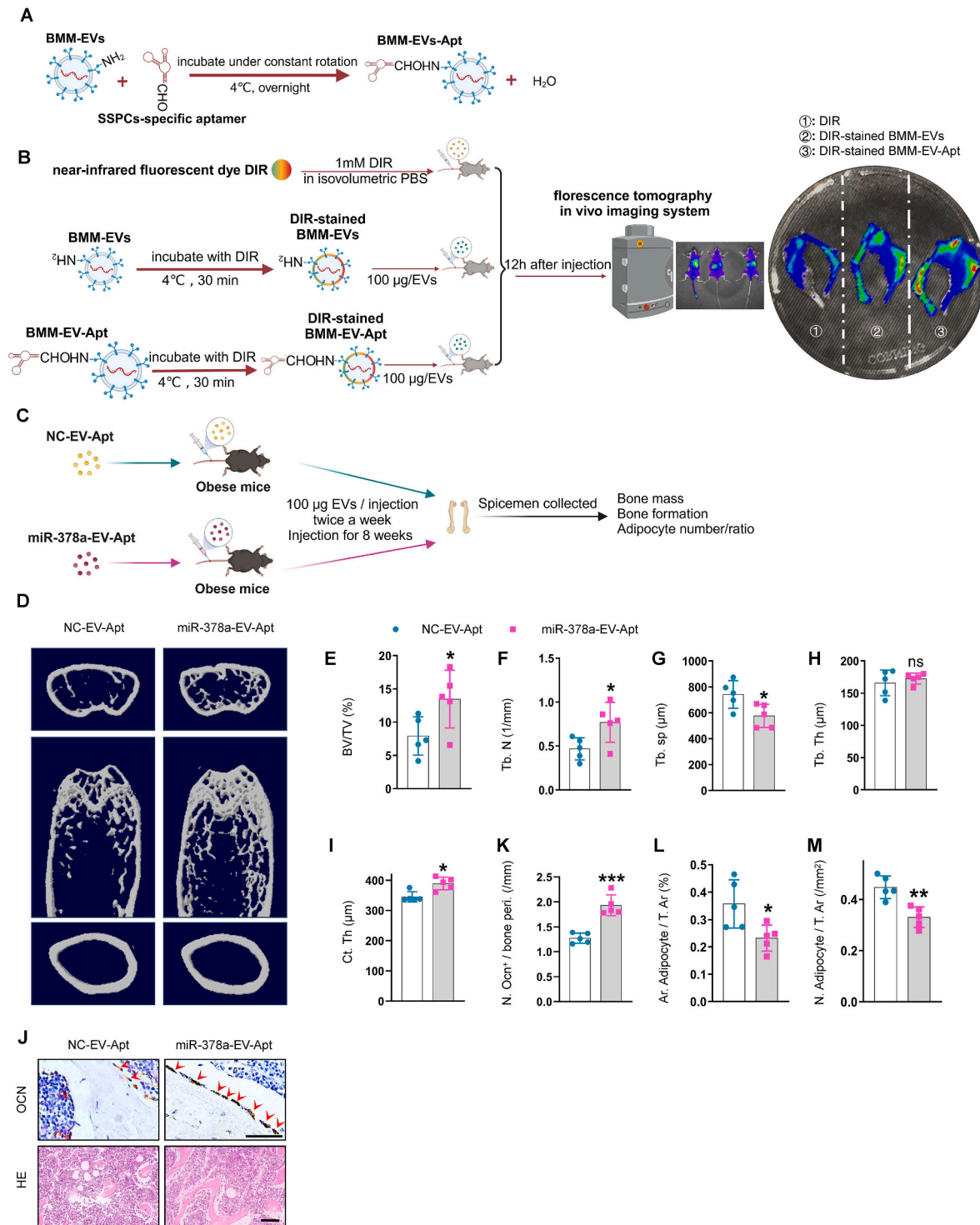
3.9. SSPC aptamer-conjugated miR-378a-overloaded extracellular vesicles alleviate bone loss in obese mice

The finding that overexpressing miR-378a via the intramedullary injection of AAV-miR-378a-3p-EGFP mitigated marrow fat accumulation in obese mice prompted us to explore a better clinical translational strategy for treating obesity-induced bone deterioration. Extracellular vesicle-drug delivery systems have attracted much attention recently due to their low immunogenicity and high stability. We tested whether miR-378a-overloaded BMM-EVs conjugated with an SSPC-targeted delivery system could rescue bone loss in obese mice. First, we used an aptamer that showed high affinity for SSPCs in a previous study [14,30] and tested the efficiency of aptamer-conjugated BMM-EVs (BMM-EV-Apt) in targeting SSPCs by injecting DIR-stained BMM-EV-Apt via the tail vein. We observed more DIR signals in the femurs of the BMM-EV-Apt-treated group than in the femurs of the BMM-EV-treated control group, suggesting that BMM-Exo-Apt efficiently targeted bone *in vivo* (Fig. 7, A and B). Then, we constructed an SSPC aptamer-conjugated miR-378a-overloaded-BMM-EV compound (miR-378a-EV-Apt) to precisely target SSPCs *in vivo*. We injected miR-378a-EV-Apt into obese mice (100 μg, twice a week for two months) (Fig. 7, C). Micro-CT analysis revealed higher trabecular bone volume and trabecular bone number and less trabecular bone separation in obese mice treated with miR-378a-EV-Apt than in obese mice treated with controls (NC-EV-Apt) (Fig. 7, D-I). In addition, the number of osteoblasts on the bone surface was greater and the number of adipocytes in the bone marrow was lower in miR-378a-EV-Apt-treated obese mice than in control mice (Fig. 7, J-M). These results suggest that overexpressing miR-378a via an extracellular-vesicle delivery system may be a precise treatment for obesity-induced bone deterioration and marrow fat accumulation and may improve bone quality in clinically obese and overweight patients.

4. Discussion

In this study, we showed that bone marrow macrophages in obese mice secrete microRNA-containing extracellular vesicles (BMM-EVs), which caused bone deterioration in lean mice. In contrast, BMM-EVs derived from lean mice ameliorated bone loss in obese recipients. miR-140 (an upregulated microRNA that promotes adipogenesis) and miR-378a (a downregulated microRNA that promotes osteogenesis) in obese BMM-EVs synergistically regulated SSPC function via the Pparα-Abca1 axis. BMM miR-140 conditional knockout mice showed resistance to obesity-induced bone deterioration. SSPC miR-140 conditional overexpression mice and BMM miR-378a conditional knockout exhibited low bone mass and marrow fat accumulation. Furthermore, SSPC-targeted miR-378a-EV-Apt increased the trabecular bone volume and trabecular bone number and decreased marrow fat accumulation in obese mice.

Obesity-induced chronic inflammation is a hallmark of multiple metabolic diseases, such as diabetes mellitus, cardiovascular disease (CVD), nonalcoholic steatohepatitis (NASH), and even cancer [18, 38–40]. In addition, chronic low-grade inflammation is a typical characteristic of aging. Previously, Li et al. reported that aging-related chronic inflammation may mediate skeletal aging through senescent bone marrow macrophages [9]. In this study, we found that extracellular vesicles act as important mediators of bone marrow macrophages in

Fig. 7. SSPC-aptamer conjugated miR-378a-overloaded-EVs alleviated bone loss in obese mice.
(A) Schematic of SSPC-aptamer conjugated BMM-EVs generation. (B) Representative fluorescence molecular tomography (FMT) images of near-infrared fluorescence signals in lower limbs isolated from mice administered with DIR dye alone, DIR-stained BMM-EV, and DIR-stained aptamer-conjugated BMM-EVs (BMM-EV-apt). (C) Schematic of SSPC-aptamer conjugated miR-378a-BMM-EV generation. (D-I) Representative μCT images (D) and quantitative μCT analysis of trabecular (E-H) and cortical bone (I) from obese mice with NC-EV-Apt and/or miR-378a-EV-Apt intervention. (J) Representative images of osteocalcin staining (J, top). Red arrows mark osteoblasts. Scale bar: 50 μm; representative images of H&E staining (J, bottom). Scale bar: 100 μm (K–M) Quantification of number of osteoblasts (K) and number and area of adipocytes (L–M). Data is shown as mean ± SD. *$P < 0.05$, **$P < 0.01$, ***$P < 0.001$, ns, no significant. (Non-parametric test is used in Fig. 7 I, and student *t*-test is used in others).

obese mice and promote bone deterioration and marrow fat accumulation. The bone phenotype of HFD-induced obese mice is similar to that of naturally aging mice in previous studies, i.e., skeletal exhibits bone loss and marrow fat accumulation [9,13,41,42]. Extracellular vesicles are widely studied, carrying and protecting numerous cargoes against degradation in circulation. Furthermore, extracellular vesicles have tremendous therapeutic potential as drug payloads with low immunogenicity, minimal clearance, low toxicity, and good tolerability. Given that macrophages and macrophage-derived extracellular vesicles are involved in diverse metabolic and aging-related diseases, targeting or modifying BMM-EVs may constitute a novel treatment strategy not only for obesity-induced bone deterioration but also for CVD, NASH, cancer, tumorigenesis, metabolic disorders, and age-related diseases.

Although the effects of obesity on bone mass are complex and controversial in clinical studies due to various factors, such as mechanical loading, obesity type, adipose tissue location, sex, age, and skeleton type, the osteoporotic bone phenotype is quite consistent in long-term high-fat diet-induced obese animal models [43–46]. In addition, data from epidemiological studies strongly suggest that obesity increases fracture risk despite a standard or high BMD, indicating the negative effect of obesity on bone health and quality. In this study, we selected the HFD model based on Shu, L. et al., who observed bone loss after 6 weeks of HFD feeding in young male mice (5 weeks old) and alterations in the bone marrow environment [43]. We fed 5-week-old male C57BL/6J mice a high-fat diet (a high-fat diet containing 60 % Kcal energy) for 8–16 weeks and observed low bone mass and marrow adiposity, which is consistent with the findings of Shu, L. et al. [43].

Extracellular vesicles provide stable cargo transportation, including proteins, mRNAs, and miRNAs transportation. miRNAs are the most numerous cargo molecules in extracellular vesicles. In our study, we found more than 1888 differentially expressed microRNAs between obese and lean BMM-EVs. Among these differentially expressed microRNAs, we screened three upregulated and three downregulated microRNAs and eventually selected miR-140 and miR-378a for study. Our data from *in vitro* and *in vivo* studies showed that a higher level of miR-140 and a lower level of miR-378a in obese BMM-EVs account for obesity-triggered bone deterioration and SSPC differentiation toward adipocytes. In addition, we found that the target genes of miR-378a and miR-140, Pparα and Abca1, belong to the same pathway. Thus, we speculate that miR-378a and miR-140 coordinately regulate bone homeostasis via the Pparα-Abca1 axis. Interestingly, the miRNA subtypes we identified in BMM-EVs did not align with those identified in adipose tissue. Data from Ying's study showed that miR-155 is enriched in obese adipose tissue macrophage-derived extracellular vesicles (ATM-EVs) and has robust effects on insulin sensitivity [18]; however, we did not observe a significant difference in miR-155 between obese and lean BMM-EVs, which implies that macrophages from different tissues secrete distinguished microRNA-containing extracellular vesicles.

miR-378a is a microRNA that plays diverse roles in pathological processes, including hepatic inflammation, bile acid metabolism, cardiac hypertrophy, and skeletal muscle metabolism [47–50]. miR-140 is reportedly involved in various diseases, such as osteoarthritis, renal fibrosis, and multiple neoplasia [51,52]. Both miR-378a and miR-140 have been reported to regulate cell proliferation, the cell cycle, and apoptosis; in addition, they also play essential roles in regulating cell differentiation. Several previous studies have reported the effects of miR-378a on osteogenesis. Specifically, You et al. reported that the overexpression of miR-378 ameliorates high glucose-induced suppression of osteogenic differentiation by activating the PI3K/Akt signaling pathway [53]. Kang et al. reported that miR-378a-enriched extracellular vesicles from M2 macrophages could promote bone repair/regeneration [54]. However, Feng et al. reported that global miR-378 transgenic mice show reduced cancellous bone mass and delayed fracture healing compared to wild-type control mice [55], which is inconsistent with our result. We speculate that the explanation for the contrary results is that, miR-378a has strong effects not only on bone but also on other tissues

and cells; the global overexpression of miR-378a in mice may disrupt homeostasis and consequently impair osteogenesis and bone formation. In addition, miR-140 has been reported to inhibit osteogenesis [56]; however, the role of miR-140 in obesity-related bone deterioration and SSPC dysfunction remains unknown. Herein, in our study, we generated transgenic mouse models with conditional knockout of miR-140 in BMMs and conditional overexpression of miR-140 in SSPCs and reported the bone phenotype of these mice for the first time. In addition, to our knowledge, this is the first report of the bone phenotype of transgenic mice with BMMs conditional knockout of miR-378a.

To translate our findings into clinical practice, we used an aptamer, which is an effective drug delivery vehicle, to enhance the efficacy and safety of therapeutic drugs for specific cell types. Previously, Li et al. conjugated antagomiR-188 with an SSPC-specific aptamer and successfully rescued age-related bone loss by precisely targeting SSPCs [14]. Aptamer-conjugated extracellular vesicle drug delivery systems exhibit unlimited therapeutic potential for bone disease. Herein, we found that treating obese recipients with a modified SSPC-specific aptamer, which delivered miR-378a-overloaded BMM-EVs, had rejuvenating effects and a robust improvement in bone mass. Based on the positive therapeutic effect of miR-378a-EV-Apt on bone loss in obese mice, targeting miR-378a in SSPCs may offer a novel treatment strategy not only for obesity-induced bone deterioration but also for SSPC-based diseases such as osteoporosis and bone fracture.

5. Limitations

One limitation of this study is that we screened 1888 differentially expressed microRNAs between obese macrophage extracellular vesicles and lean macrophage extracellular vesicles and found that miR-140 and miR-378a coordinately regulated SSPC function; however, we did not test whether other microRNAs may also mediate the effects of BMM-EVs on bone. Another limitation is that we only measured the effects of BMM-EVs on bone in mice. We realize that there is a large gap between humans and rodents in terms of the physiological and pathological functions of BMMs and BMM-EVs. The direct effects of BMMs and BMM-EVs isolated from human patients with obesity on bone should be tested in future studies. Despite these limitations, our study revealed that obesity triggers changes in BMM-secreted microRNA-containing extracellular vesicles, disrupts SSPC function, and exacerbates bone deterioration; these findings reveal that BMM-EVs and aptamer-conjugated BMM-EVs show great therapeutic potential because of their low immunogenicity, minimal clearance, and cell-targeting ability in preventing not only obesity-related bone deterioration but also shed light on treating age-related osteoporosis and other chronic inflammation-induced diseases.

Ethics approval and consent to participate

The experimental design followed the "3 R" principle. All mice we used were in C57 BL/6J background and were maintained in a standard, specific pathogen-free barrier of Department of Animals Laboratory, Central South University with 12 light/12 dark cycles and 4–5 mice per cage. All the experimental protocols were approved by the Animal Care and Use Committees of the Laboratory Animal Research Center at Xiangya Medical School of Central South University. All the authors listed consented with all relevant ethical regulations.

Data availability statement

The data that support the findings of this study are available within the article and its supplementary materials or from the corresponding author upon reasonable request.

CRediT authorship contribution statement

Declaration of Competing interest

The authors declare no conflict of interests.

Acknowledgement

Appendix A. Supplementary data

Supplementary data to this article can be found online at https://doi.org/10.1016/j.bioactmat.2024.06.035.

References

[1] M. Hata, E. Andriessen, M. Hata, R. Diaz-Marin, F. Fournier, S. Crespo-Garcia, G. Blot, R. Juneau, F. Pilon, A. Dejda, V. Guber, E. Heckel, C. Daneault, V. Calderon, C. Des Rosiers, H.J. Melichar, T. Langmann, J.S. Joyal, A.M. Wilson, P. Sapieha, Past history of obesity triggers persistent epigenetic changes in innate immunity and exacerbates neuroinflammation, Science 379 (6627) (2023) 45–62, https://doi.org/10.1126/science.abj8894.

[2] S.P. Bapat, C. Whitty, C.T. Mowery, Y. Liang, A. Yoo, Z. Jiang, M.C. Peters, L. J. Zhang, I. Vogel, C. Zhou, V.Q. Nguyen, Z. Li, C. Chang, W.S. Zhu, A.T. Hastie, H. He, X. Ren, W. Qiu, S.G. Gayer, C. Liu, E.J. Choi, M. Fassett, J.N. Cohen, J. L. Sturgill, L.E. Crotty Alexander, J.M. Suh, C. Liddle, A.R. Atkins, R.T. Yu, M. Downes, S. Liu, B.S. Nikolajczyk, I.K. Lee, E. Guttman-Yassky, K.M. Ansel, P. G. Woodruff, J.V. Fahy, D. Sheppard, R.L. Gallo, C.J. Ye, R.M. Evans, Y. Zheng, A. Marson, Obesity alters pathology and treatment response in inflammatory disease, Nature 604 (7905) (2022) 337–342, https://doi.org/10.1038/s41586-022-04536-0.

[3] Q. Li, C.E. Hagberg, H. Silva Cascales, S. Lang, M.T. Hyvonen, F. Salehzadeh, P. Chen, I. Alexandersson, E. Terezaki, M.J. Harms, M. Kutschke, N. Arifen, N. Kramer, M. Aouadi, C. Knibbe, J. Boucher, A. Thorell, K.L. Spalding, Obesity and hyperinsulinemia drive adipocytes to activate a cell cycle program and senesce, Nat Med 27 (11) (2021) 1941–1953, https://doi.org/10.1038/s41591-021-01501-8.

[4] F. Cardoso, R.G.J. Klein Wolterink, C. Godinho-Silva, R.G. Domingues, H. Ribeiro, J.A. da Silva, I. Mahu, A.I. Domingos, H. Veiga-Fernandes, Neuro-mesenchymal units control ILC2 and obesity via a brain-adipose circuit, Nature 597 (7876) (2021) 410–414, https://doi.org/10.1038/s41586-021-03830-7.

[5] P. Zhang, M. Peterson, G.L. Su, S.C. Wang, Visceral adiposity is negatively associated with bone density and muscle attenuation, Am. J. Clin. Nutr. 101 (2) (2015) 337–343, https://doi.org/10.3945/ajcn.113.081778.

[6] B. Dai, J. Xu, X. Li, L. Huang, C. Hopkins, H. Wang, H. Yao, J. Mi, L. Zheng, J. Wang, W. Tong, D.H. Chow, Y. Li, X. He, P. Hu, Z. Chen, H. Zu, Y. Li, Y. Yao, Q. Jiang, L. Qin, Macrophages in epididymal adipose tissue secrete osteopontin to regulate bone homeostasis, Nat. Commun. 13 (1) (2022) 427, https://doi.org/10.1038/s41467-021-27683-w.

[7] H. Zahedi, F. Atayie, F. Samii Kondrud, A. Balali, J. Beyene, N. Tahery, M. Asadi, O. Sadeghi, Associations of abdominal obesity with different types of bone fractures in adults: a systematic review and dose-response meta-analysis of prospective cohort studies, Crit. Rev. Food Sci. Nutr. (2023) 1–12, https://doi.org/10.1080/10408398.2023.2166456.

[8] M. Tencerova, F. Figeac, N. Ditzel, H. Taipaleenmaki, T.K. Nielsen, M. Kassem, High-fat diet-induced obesity promotes Expansion of bone marrow adipose tissue and impairs skeletal stem cell functions in mice, J. Bone Miner. Res. 33 (6) (2018) 1154–1165, https://doi.org/10.1002/jbmr.3408.

[9] C.J. Li, Y. Xiao, Y.C. Sun, W.Z. He, L. Liu, M. Huang, C. He, M. Huang, K.X. Chen, J. Hou, X. Feng, T. Su, Q. Guo, Y. Huang, H. Peng, M. Yang, G.H. Liu, X.H. Luo, Senescent immune cells release grancalcin to promote skeletal aging, Cell Metab 33 (10) (2021) 1957–1973 e6, https://doi.org/10.1016/j.cmet.2021.08.009.

[10] Q. Sun, Y. Hou, Z. Chu, Q. Wei, Soft overcomes the hard: Flexible materials adapt to cell adhesion to promote cell mechanotransduction, Bioact. Mater. 10 (2022) 397–404, https://doi.org/10.1016/j.bioactmat.2021.08.026.

[11] W. Xie, X. Wei, H. Kang, H. Jiang, Z. Chu, Y. Lin, Y. Hou, Q. Wei, Static and Dynamic: Evolving biomaterial mechanical Properties to control Cellular mechanotransduction, Adv. Sci. 10 (9) (2023) e2204594, https://doi.org/10.1002/advs.202204594.

[12] Y. Li, L. Lu, Y. Xie, X. Chen, L. Tian, Y. Liang, H. Li, J. Zhang, Y. Liu, X. Yu, Interleukin-6 knockout inhibits senescence of bone mesenchymal stem cells in high-fat diet-induced bone loss, Front. Endocrinol. 11 (2020) 622950, https://doi.org/10.3389/fendo.2020.622950.

[13] C.J. Li, Y. Xiao, M. Yang, T. Su, X. Sun, Q. Guo, Y. Huang, X.H. Luo, Long noncoding RNA Bmncr regulates mesenchymal stem cell fate during skeletal aging, J. Clin. Invest. 128 (12) (2018) 5251–5266, https://doi.org/10.1172/JCI99044.

[14] C.J. Li, P. Cheng, M.K. Liang, Y.S. Chen, Q. Lu, J.Y. Wang, Z.Y. Xia, H.D. Zhou, X. Cao, H. Xie, E.Y. Liao, X.H. Luo, MicroRNA-188 regulates age-related switch between osteoblast and adipocyte differentiation, J. Clin. Invest. 125 (4) (2015) 1509–1522, https://doi.org/10.1172/JCI77116.

[15] W. Zou, N. Rohatgi, J.R. Brestoff, Y. Li, R.A. Barve, E. Tycksen, Y. Kim, M.J. Silva, S.L. Teitelbaum, Ablation of fat cells in adult mice induces massive bone Gain, Cell Metab 32 (5) (2020) 801–813 e6, https://doi.org/10.1016/j.cmet.2020.09.011.

[16] T.H. Ambrosi, A. Scialdone, A. Graja, S. Gohlke, A.M. Jank, C. Bocian, L. Woelk, H. Fan, D.W. Logan, A. Schurmann, L.R. Saraiva, T.J. Schulz, Adipocyte accumulation in the bone marrow during obesity and aging impairs stem cell-based hematopoietic and bone regeneration, Cell Stem Cell 20 (6) (2017) 771–784 e6, https://doi.org/10.1016/j.stem.2017.02.009.

[17] W. Ying, H. Gao, F.C.G. Dos Reis, G. Bandyopadhyay, J.M. Ofrecio, Z. Luo, Y. Ji, Z. Jin, C. Ly, J.M. Olefsky, MiR-690, an exosomal-derived miRNA from M2-polarized macrophages, improves insulin sensitivity in obese mice, Cell Metab 33 (4) (2021) 781–790 e5, https://doi.org/10.1016/j.cmet.2020.12.019.

[18] W. Ying, M. Riopel, G. Bandyopadhyay, Y. Dong, A. Birmingham, J.B. Seo, J. M. Ofrecio, J. Wollam, A. Hernandez-Carretero, W. Fu, P. Li, J.M. Olefsky, Adipose tissue macrophage-derived exosomal miRNAs can modulate in vivo and in vitro insulin sensitivity, Cell 171 (2) (2017) 372–384 e12, https://doi.org/10.1016/j.cell.2017.08.035.

[19] B.C. Lee, M.S. Kim, M. Pae, Y. Yamamoto, D. Eberle, T. Shimada, N. Kamei, H. S. Park, S. Sasorith, J.R. Woo, J. You, W. Mosher, H.J. Brady, S.E. Shoelson, J. Lee, Adipose natural Killer cells regulate adipose tissue macrophages to promote insulin resistance in obesity, Cell Metab 23 (4) (2016) 685–698, https://doi.org/10.1016/j.cmet.2016.03.002.

[20] R. Kalluri, V.S. LeBleu, The biology, function, and biomedical applications of exosomes, Science 367 (6478) (2020), https://doi.org/10.1126/science.aau6977.

[21] C.H. Hu, B.D. Sui, J. Liu, L. Dang, J. Chen, C.X. Zheng, S. Shi, N. Zhao, M.Y. Dang, X.N. He, L.Q. Zhang, P.P. Gao, N. Chen, H.J. Kuang, K. Chen, X.L. Xu, X.R. Yu, G. Zhang, Y. Jin, Sympathetic Neurostress Drives osteoblastic exosomal MiR-21 transfer to disrupt bone homeostasis and promote Osteopenia, Small Methods 6 (3) (2022) e2100763, https://doi.org/10.1002/smtd.202100763.

[22] D.K. Kim, G. Bandara, Y.E. Cho, H.D. Komarow, D.R. Donahue, B. Karim, M. C. Baek, H.M. Kim, D.D. Metcalfe, A. Olivera, Mastocytosis-derived extracellular vesicles deliver miR-23a and miR-30a into pre-osteoblasts and prevent osteoblastogenesis and bone formation, Nat. Commun. 12 (1) (2021) 2527, https://doi.org/10.1038/s41467-021-22754-4.

[23] H. Hu, L. Dong, Z. Bu, Y. Shen, J. Luo, H. Zhang, S. Zhao, F. Lv, Z. Liu, miR-23a-3p-abundant small extracellular vesicles released from Gelma/nanoclay hydrogel for cartilage regeneration, J. Extracell. Vesicles 9 (1) (2020) 1778883, https://doi.org/10.1080/20013078.2020.1778883.

[24] S. Bheri, M.E. Brown, H.J. Park, O. Brazhkina, F. Takaesu, M.E. Davis, Customized loading of microRNA-126 to small extracellular vesicle-derived vehicles improves cardiac function after Myocardial Infarction, ACS Nano 17 (20) (2023) 19613–19624, https://doi.org/10.1021/acsnano.3c01534.

[25] Y. Ji, Z. Luo, H. Gao, F.C.G. Dos Reis, G. Bandyopadhyay, Z. Jin, K.A. Manda, R. Isaac, M. Yang, W. Fu, W. Ying, J.M. Olefsky, Hepatocyte-derived exosomes from early onset obese mice promote insulin sensitivity through miR-3075, Nat. Metab. 3 (9) (2021) 1163–1174, https://doi.org/10.1038/s42255-021-00444-1.

[26] B. Peruzzi, E. Urciuoli, M. Mariani, L. Chioma, L. Tomao, I. Montano, M. Algeri, R. Luciano, D. Fintini, M. Manco, Circulating extracellular vesicles impair mesenchymal stromal cell differentiation favoring adipogenic rather than osteogenic differentiation in adolescents with obesity, Int. J. Mol. Sci. 24 (1) (2022), https://doi.org/10.3390/ijms24010447.

[27] D. Zhang, Y. Wu, Z. Li, H. Chen, S. Huang, C. Jian, A. Yu, MiR-144-5p, an exosomal miRNA from bone marrow-derived macrophage in type 2 diabetes, impairs bone fracture healing via targeting Smad1, J Nanobiotechnology 19 (1) (2021) 226, https://doi.org/10.1186/s12951-021-00964-8.

[28] M. Panigaj, M.B. Johnson, W. Ke, J. McMillan, E.A. Goncharova, M. Chandler, K. A. Afonin, Aptamers as modular components of therapeutic Nucleic acid Nanotechnology, ACS Nano 13 (11) (2019) 12301–12321, https://doi.org/10.1021/acsnano.9b06522.

[29] E.S. Gragoudas, A.P. Adamis, E.T. Cunningham Jr., M. Feinsod, D.R. Guyer; VEGF Inhibition Study in Ocular Neovascularization Clinical Trial Group, Pegaptanib for neovascular age-related macular degeneration, N. Engl. J. Med. 351 (27) (2004) 2805–2816, doi:10.1056/NEJMoa042760.

[30] Z.W. Luo, F.X. Li, Y.W. Liu, S.S. Rao, H. Yin, J. Huang, C.Y. Chen, Y. Hu, Y. Zhang, Y.J. Tan, L.Q. Yuan, T.H. Chen, H.M. Liu, J. Cao, Z.Z. Liu, Z.X. Wang, H. Xie, Aptamer-functionalized exosomes from bone marrow stromal cells target bone to promote bone regeneration, Nanoscale 11 (43) (2019) 20884–20892, https://doi.org/10.1039/c9nr02791b.

[31] J. Shou, S. Li, W. Shi, S. Zhang, Z. Zeng, Z. Guo, Z. Ye, Z. Wen, H. Qiu, J. Wang, M. Zhou, 3WJ RNA Nanoparticles-aptamer functionalized exosomes from M2 macrophages target BMSCs to promote the healing of bone fractures, Stem Cells Transl Med 12 (11) (2023) 758–774, https://doi.org/10.1093/stcltm/szad052.

[32] Y. Su, Q. Gao, R. Deng, L. Zeng, J. Guo, B. Ye, J. Yu, X. Guo, Aptamer engineering exosomes loaded on biomimetic periosteum to promote angiogenesis and bone regeneration by targeting injured nerves via JNK3 MAPK pathway, Mater Today Bio 16 (2022) 100434, https://doi.org/10.1016/j.mtbio.2022.100434.

[33] P.H. Tran, D. Xiang, T.N. Nguyen, T.T. Tran, Q. Chen, W. Yin, Y. Zhang, L. Kong, A. Duan, K. Chen, M. Sun, Y. Li, Y. Hou, Y. Zhu, Y. Ma, G. Jiang, W. Duan, Aptamer-guided extracellular vesicle theranostics in oncology, Theranostics 10 (9) (2020) 3849–3866, https://doi.org/10.7150/thno.39706.

[34] W.Z. He, M. Yang, Y. Jiang, C. He, Y.C. Sun, L. Liu, M. Huang, Y.R. Jiao, K.X. Chen, J. Hou, M. Huang, Y.L. Xu, X. Feng, Y. Liu, Q. Guo, H. Peng, Y. Huang, T. Su, Y. Xiao, Y. Li, C. Zeng, G. Lei, X.H. Luo, C.J. Li, miR-188-3p targets skeletal endothelium coupling of angiogenesis and osteogenesis during ageing, Cell Death Dis. 13 (5) (2022) 494, https://doi.org/10.1038/s41419-022-04902-w.

[35] T. Su, Y. Xiao, Y. Xiao, Q. Guo, C. Li, Y. Huang, Q. Deng, J. Wen, F. Zhou, X.H. Luo, Bone marrow mesenchymal stem cells-derived exosomal MiR-29b-3p regulates aging-associated insulin resistance, ACS Nano 13 (2) (2019) 2450–2462, https://doi.org/10.1021/acsnano.8b09375.

[36] Y. Zheng, Y. Xiao, D. Zhang, S. Zhang, J. Ouyang, L. Li, W. Shi, R. Zhang, H. Liu, Q. Jin, Z. Chen, D. Xu, L. Wu, Geniposide ameliorated dexamethasone-induced cholesterol accumulation in osteoblasts by mediating the GLP-1R/ABCA1 Axis, Cells 10 (12) (2021), https://doi.org/10.3390/cells10123424.

[37] T.D. Hinds Jr., Z.A. Kipp, M. Xu, F.B. Yiannikouris, A.J. Morris, D.F. Stec, W. Wahli, D.E. Stec, Adipose-specific PPARalpha knockout mice have increased Lipogenesis by PASK-SREBP1 signaling and a Polarity Shift to inflammatory macrophages in white adipose tissue, Cells 11 (1) (2021), https://doi.org/10.3390/cells11010004.

[38] M. Bijnen, T. Josefs, I. Cuijpers, C.J. Maalsen, J. van de Gaar, M. Vroomen, E. Wijnands, S.S. Rensen, J.W.M. Greve, M.H. Hofker, E.A.L. Biessen, C.D. A. Stehouwer, C.G. Schalkwijk, K. Wouters, Adipose tissue macrophages induce hepatic neutrophil recruitment and macrophage accumulation in mice, Gut 67 (7) (2018) 1317–1327, https://doi.org/10.1136/gutjnl-2016-313654.

[39] J. Song, D. Farris, P. Ariza, S. Moorjani, M. Varghese, M. Blin, J. Chen, D. Tyrrell, M. Zhang, K. Singer, M. Salmon, D.R. Goldstein, Age-associated adipose tissue inflammation promotes monocyte chemotaxis and enhances atherosclerosis, Aging Cell 22 (2) (2023) e13783, https://doi.org/10.1111/acel.13783.

[40] V. Laurent, A. Guerard, C. Mazerolles, S. Le Gonidec, A. Toulet, L. Nieto, F. Zaidi, B. Majed, D. Garandeau, Y. Socrier, M. Golzio, T. Cadoudal, K. Chaoui, C. Dray, B. Monsarrat, O. Schiltz, Y.Y. Wang, B. Couderc, P. Valet, B. Malavaud, C. Muller, Periprostatic adipocytes act as a driving force for prostate cancer progression in obesity, Nat. Commun. 7 (2016) 10230, https://doi.org/10.1038/ncomms10230.

[41] W. Ling, K. Krager, K.K. Richardson, A.D. Warren, F. Ponte, N. Aykin-Burns, S. C. Manolagas, M. Almeida, H.N. Kim, Mitochondrial Sirt3 contributes to the bone loss caused by aging or estrogen deficiency, JCI Insight 6 (10) (2021), https://doi.org/10.1172/jci.insight.146728.

[42] M. Yang, C.J. Li, X. Sun, Q. Guo, Y. Xiao, T. Su, M.L. Tu, H. Peng, Q. Lu, Q. Liu, H. B. He, T.J. Jiang, M.X. Lei, M. Wan, X. Cao, X.H. Luo, MiR-497 approximately 195 cluster regulates angiogenesis during coupling with osteogenesis by maintaining endothelial Notch and HIF-1alpha activity, Nat. Commun. 8 (2017) 16003, https://doi.org/10.1038/ncomms16003.

[43] L. Shu, E. Beier, T. Sheu, H. Zhang, M.J. Zuscik, E.J. Puzas, B.F. Boyce, R. A. Mooney, L. Xing, High-fat diet causes bone loss in young mice by promoting osteoclastogenesis through alteration of the bone marrow environment, Calcif. Tissue Int. 96 (4) (2015) 313–323, https://doi.org/10.1007/s00223-015-9954-z.

[44] Y. Peng, J. Liu, Y. Tang, J. Liu, T. Han, S. Han, H. Li, C. Hou, J. Liu, J. Long, High-fat-diet-induced weight Gain ameliorates bone loss without exacerbating AbetaPP processing and Cognition in Female APP/PS1 mice, Front. Cell. Neurosci. 8 (2014) 225, https://doi.org/10.3389/fncel.2014.00225.

[45] J. Hou, C. He, W. He, M. Yang, X. Luo, C. Li, Obesity and bone health: a complex Link, Front. Cell Dev. Biol. 8 (2020) 600181, https://doi.org/10.3389/fcell.2020.600181.

[46] S.A. Shapses, L.C. Pop, Y. Wang, Obesity is a concern for bone health with aging, Nutr. Res. 39 (2017) 1–13, https://doi.org/10.1016/j.nutres.2016.12.010.

[47] T. Zhang, J. Hu, X. Wang, X. Zhao, Z. Li, J. Niu, C.J. Steer, G. Zheng, G. Song, MicroRNA-378 promotes hepatic inflammation and fibrosis via modulation of the NF-kappaB-TNFalpha pathway, J. Hepatol. 70 (1) (2019) 87–96, https://doi.org/10.1016/j.jhep.2018.08.026.

[48] C. Sun, W. Liu, Z. Lu, Y. Li, S. Liu, Z. Tang, Y. Yan, Z. Li, H. Feng, D. Zhang, Y. Liu, Z.Z. Fang, C. Jiang, Q. Ding, J. Jiang, H. Ying, Hepatic miR-378 modulates serum cholesterol levels by regulating hepatic bile acid synthesis, Theranostics 11 (9) (2021) 4363–4380, https://doi.org/10.7150/thno.53624.

[49] J. Ganesan, D. Ramanujam, Y. Sassi, A. Ahles, C. Jentzsch, S. Werfel, S. Leierseder, X. Loyer, M. Giacca, L. Zentilin, T. Thum, B. Laggerbauer, S. Engelhardt, MiR-378 controls cardiac hypertrophy by combined repression of mitogen-activated protein kinase pathway factors, Circulation 127 (21) (2013) 2097–2106, https://doi.org/10.1161/CIRCULATIONAHA.112.000882.

[50] Y. Li, J. Jiang, W. Liu, H. Wang, L. Zhao, S. Liu, P. Li, S. Zhang, C. Sun, Y. Wu, S. Yu, X. Li, H. Zhang, H. Qian, D. Zhang, F. Guo, Q. Zhai, Q. Ding, L. Wang, H. Ying, microRNA-378 promotes autophagy and inhibits apoptosis in skeletal muscle, Proc Natl Acad Sci U S A 115 (46) (2018) E10849–E10858, https://doi.org/10.1073/pnas.1803377115.

[51] H.B. Si, T.M. Yang, L. Li, M. Tian, L. Zhou, D.P. Li, Q. Huang, P.D. Kang, J. Yang, Z. K. Zhou, J.Q. Cheng, B. Shen, miR-140 attenuates the progression of early-Stage osteoarthritis by Retarding Chondrocyte senescence, Mol. Ther. Nucleic Acids 19 (2020) 15–30, https://doi.org/10.1016/j.omtn.2019.10.032.

[52] S. Ghafouri-Fard, Z. Bahroudi, H. Shoorei, A. Abak, M. Ahin, M. Taheri, microRNA-140: a miRNA with diverse roles in human diseases, Biomed. Pharmacother. 135 (2021) 111256, https://doi.org/10.1016/j.biopha.2021.111256.

[53] L. You, W. Gu, L. Chen, L. Pan, J. Chen, Y. Peng, MiR-378 overexpression attenuates high glucose-suppressed osteogenic differentiation through targeting CASP3 and activating PI3K/Akt signaling pathway, Int. J. Clin. Exp. Pathol. 7 (10) (2014) 7249–7261.

[54] M. Kang, C.C. Huang, Y. Lu, S. Shirazi, P. Gajendrareddy, S. Ravindran, L. F. Cooper, Bone regeneration is mediated by macrophage extracellular vesicles, Bone 141 (2020) 115627, https://doi.org/10.1016/j.bone.2020.115627.

[55] L. Feng, J.F. Zhang, L. Shi, Z.M. Yang, T.Y. Wu, H.X. Wang, W.P. Lin, Y.F. Lu, J.H. T. Lo, D.H. Zhu, G. Li, MicroRNA-378 suppressed osteogenesis of MSCs and impaired bone formation via Inactivating Wnt/beta-Catenin signaling, Mol. Ther. Nucleic Acids 21 (2020) 1017–1028, https://doi.org/10.1016/j.omtn.2020.07.018.

[56] Y. Tang, Y. Sun, J. Zeng, B. Yuan, Y. Zhao, X. Geng, L. Jia, S. Zhou, X. Chen, Exosomal miR-140-5p inhibits osteogenesis by targeting IGF1R and regulating the mTOR pathway in ossification of the posterior longitudinal ligament, J Nanobiotechnology 20 (1) (2022) 452, https://doi.org/10.1186/s12951-022-01655-8.